MICROSTRUCTURAL CHARACTERISTICS AND MECHANICAL BEHAVIOR OF ANTI-CORROSIVE AL-ZN THERMAL SPRAY COATINGS DEPOSITED BY WIRE ARC SPRAYING AND COLD SPRAYING TECHNIQUES

A Thesis
Submitted to the Graduate Faculty
of the
North Dakota State University
of Agriculture and Applied Science

By

Amir Darabi Noferesti

In Partial Fulfillment of the Requirements
for the Degree of
MASTER OF SCIENCE

Major Department:
Mechanical Engineering

May 2019

Fargo, North Dakota

North Dakota State University
Graduate School

Title

Microstructural Characteristics and Mechanical Behavior of Anticorrosive Al-Zn Thermal Spray Coatings Deposited by Wire Arc Spraying and Cold Spraying Techniques

By

Amir Darabi Noferesti

The Supervisory Committee certifies that this ***disquisition*** complies with North Dakota State University's regulations and meets the accepted standards for the degree of

MASTER OF SCIENCE

SUPERVISORY COMMITTEE:

Dr. Fardad Azarmi
Chair

Dr. Ghodrat Karami

Dr. Annie Tangpong

Dr. Ying Huang

Approved:

6/12/2019 — Date

Dr. Alan Kallmeyer — Department Chair

ABSTRACT

Mechanical properties of thermal spray deposited coatings are highly influenced by their microstructural characteristics. The objective of this investigation is to evaluate the mechanical properties of thermally sprayed coatings consisted of aluminum and zinc based on the coating microstructure, using an image based computational scheme. Microstructural images of coating samples were subjected to image-based finite element analysis and the results were validated by experimental tests and analytical models. Comparison of the experimental data with FEA was used to explain the microstructural basis of the mechanical characteristics of Al-Zn coatings and the differences between two methods of thermal spray techniques. It was concluded that the cold spraying technique produces higher-quality coatings with less porosity and higher hardness compared to wire arc deposition. An isotropic behavior was observed in the cold sprayed coating. Finally, the electrochemical tests showed that the coating with a higher amount of zinc had better anti-corrosion properties.

ACKNOWLEDGEMENTS

I would like to especially thank my adviser Dr. Fardad Azarmi for providing me an opportunity to work under his supervision for the last two years and for the guidance he has shown me along the way. Furthermore, I want to thank my committee members Dr. Ghodrat Karami, Dr. Annie Tangpong, and Dr. Ying Huang for their time, patience and guidance on this project.

I would like to thank PHMSA/DOT for providing funding for this thesis project; without your investment, this research would not be possible.

I would like to acknowledge some other members and facilities of the North Dakota State University team for their assistance in this project, and also SEM Center of NDSU. I also would like to appreciate the help of Dr. Fodan Deng for conducting corrosion test on coating samples. Thank you for assistance in completing this project and helping me to learn a variety of testing techniques and research practices which have formed the basis of my research career.

DEDICATION

I want to dedicate this research to my lovely wife and best friend,

Ghazal

And to my supportive family

Thank you for your unconditional love and support.

TABLE OF CONTENTS

LIST OF TABLES

LIST OF FIGURES

LIST OF APPENDIX TABLES

LIST OF APPENDIX FIGURES

CHAPTER 1. GENERAL INTRODUCTION

Wire arc deposition method is a well know technology for production of zinc-based coatings (Zn-15Al in this study) with great anti-corrosion properties; this process is known by industry as “metallization”. It is commonly used in the pipeline industry to protect them from environmental damages such as corrosion and erosion.

This study investigates the possibility of using an alternative approach for producing protective layers by deposition of same combination of the materials but at different volume fraction (Al-25Zn) via cold spraying technique, instead of wire arc spraying.

Cold spray deposition method produces dense, high-quality coatings with a relatively small amount of porosity. The advanced cold spray equipment is compact and mobile which make them more flexible and desirable for on-site applications. Due to elimination of melting and solidification during cold spraying process, it is possible to produce thick coatings with high quality (less voids). For the same reason, oxidation is zero or minimum during cold spraying as well. Because of multiple benefits of cold spray technology, this technique is proposed as an alternative to the currently employed “Metallization” process that mainly uses wire arc deposited coatings to improve corrosion resistance of oil and gas pipelines. In addition, this study evaluates mechanical properties of cold sprayed Al-25Zn to understand its performance against Zn-15Al coating produced by metallization.

Microstructural features play an important role in the properties of the thermal spray deposits. The formation of the coating layers, the interfacial properties between the layers, and the distribution of the voids and pores in the coating microstructure can affect the behavior of the coatings and it is crucial to consider these features when different types of coatings are under investigation. As a result, the main focus of this study is to evaluate the mechanical behavior of

the coatings and find the effects of microstructural features using image-based finite element analysis.

1.1. Research Objectives

This study has two goals:

1- Finding the influence of microstructural features on the mechanical behavior of both types of coatings in this study.

2- Comparison of the coatings deposited by wire arc spray and cold spray methods in terms of microstructural characteristics, mechanical behavior, and electrochemical properties, to find the optimum deposition technique for corrosion protection of pipelines.

To achieve the above-mentioned goals, the following research objectives should be taken into account. These steps are performed on both types of coating samples.

1- Scanning Electron Microscopy (SEM) was used for microstructural characterization and observation of the distribution of different microstructural features. Elemental composition of each coating was obtained using EDS diffractometer on the SEM equipment.

2- Mechanical experiments such as nanoindentation, resonance frequency analysis, and microhardness measurements, to measure important mechanical properties of the coatings such as hardness and elastic modulus.

3- Numerical simulations on actual micrographs of the coating samples to calculate the elastic modulus. The hypothesis is that the microstructural features, such as voids, pores and splat boundaries, affect the mechanical properties of the coating.

4- Employing available analytical models to estimate mechanical properties of two-phase and porous structures (cases of coating structures).
5- A brief study of corrosion resistant properties of the coating samples to achieve a better comparison between the coatings for the energy transportation applications.

1.2. Disquisition Organization

This disquisition is written in four major chapters. The first chapter is a literature review of pipelines and thermal spray technology, with a comprehensive description of wire arc deposition and cold spray deposition techniques, which are the main deposition methods used in this study.

Chapter two focuses on the wire arc deposited Zn-15Al coating to find the effects of microstructural feature on the mechanical properties of the coating. The experimental procedures used in this study such as microstructural characterization and mechanical experiments, including microhardness, nanoindentation, and resonance frequency analysis are described in this chapter. In addition, an image-based finite element analysis was utilized to numerically simulate mechanical properties of the wire arc deposited coating based on its microstructural properties.

Chapter three investigates the microstructural and mechanical properties of the cold spray deposited Al-25Zn coating. Microstructural features of the coating were studied by scanning electron microscopy, which were later subjected to an image-based finite element analysis to determine the elastic modulus of the coating. The measured values of numerical simulation were validated by mechanical experiments such as Vickers and Knoop indentation, nanoindentation, and resonance frequency analysis.

Chapter four compares the mechanical properties as well as the corrosion resistance of the coatings from the two thermal spraying techniques utilized in this study. The results of microstructural characterization and mechanical experiments in the previous sections are used to

discuss which technique produces a higher-quality deposit. A brief discussion is made about the corrosion resistance of the coatings to investigate the possibility of replacing wire arc deposition with cold spraying as the main method for “Metallization”.

Lastly, chapter five provides the final conclusions on the comparison between the coating performances, as well as the future steps and recommendations that may help to further improve this study.

CHAPTER 2. LITERATURE REVIEW

2.1. Pipelines

One of the most reliable and efficient ways of energy transportation are pipelines. United States is highly dependent on pipelines for transportation and distribution of energy, since oil and natural gas contribute to more than 70% of the products that are transported through pipelines. Energy is of the essentials of human life, therefore, the existence and maintenance of pipelines is of high importance [1].

Various working environment such as diversity in weather condition all around the US has led to different problems and has shorten the service life of pipelines [2]. However, the number one cause of failure in pipeline industry of the US has proven to be corrosion [3]. Pipelines, immersed in water or buried in the ground, are susceptible to corrosion and will eventually deteriorate if proper maintenance and protection has not been performed. Corroded pipelines are weak and can lead to catastrophic accidents if hazardous materials are in transition.

Oil and gas pipelines play a significant role in energy transportation of the United States and it is of utmost importance to have a long service life or to be repaired and properly maintained during their service period. Application of anti-corrosion coatings is one of the most effective methods to protect pipelines against corrosion and its devastating consequences.

2.2. Corrosion and Mitigation

Corrosion is a chemical or electrochemical process which may lead to loss of material over a certain period of time [4]. In other words, electrochemical corrosion is caused by a flow of electricity from one metal to another, or from one part of metal to another part. This process occurs where a corroding medium exists in a liquid, gas, or solid. There are a couple of methods to mitigate corrosion, such as cathodic protection and application of a protective coating. The latter

is most commonly used by the industry. Epoxy coatings are ideal against corrosion and are used in many industries [5]. However, lack of mechanical strength has limited the use of epoxy coatings when this type of coating is subjected to mechanical loadings and deformations. Mechanical failures of epoxy coatings are mostly due to the large deformations and separation of coating from substrate, or due to low wear resistance of coating. Failure of epoxy coatings would eventually expose the substrate to the surrounding environment, resulting in corrosion formation and propagation. Therefore, coatings require a sufficient mechanical strength to prevent corrosion initiation on the surface of the substrate that they are protecting.

It is speculated that anti-corrosive metallic coatings will perform much better than epoxy coatings due to their superior mechanical properties. Zinc and aluminum are among the well-known metals in terms of corrosion resistance and zinc aluminum mixture have been used as the coating material for anti-corrosion applications in industry [6].

2.3. Thermal Spraying Techniques

Thermal spraying is a general name for a group of advanced methods for depositing protective layers on the surface of engineering parts, components, and structures. Coatings deposited by the thermal spraying techniques are increasingly finding application in aerospace, automotive, biomedical, electrical, and turbine industries [7].

Thermal spraying processes improve the performance of a substrate or a component by applying coatings layer by layer on the industrial surfaces. A wide range of materials, including ceramics, alloys, metals, some type of polymers and carbides can be deposited using thermal spraying techniques. These coatings can provide protection from corrosion, wear, erosion, and excessive temperature. Thermal spraying methods can be divided into two major categories based on energy source [8]. Combustion by different types of fuels or electrical current are two major

energy sources for thermal spraying technologies. The energy is used to heat the coating material, in shape of wire or powder, to a molten or semi molten state. Next, the molten particles are accelerated towards the substrate. Upon impact, a mechanical or metallurgical bond forms between the particles and the substrate, and the high cooling rate helps the solidification of particles, leading to the formation of the coating build up on the surface. Figure 2-1 shows the step by step deposition process.

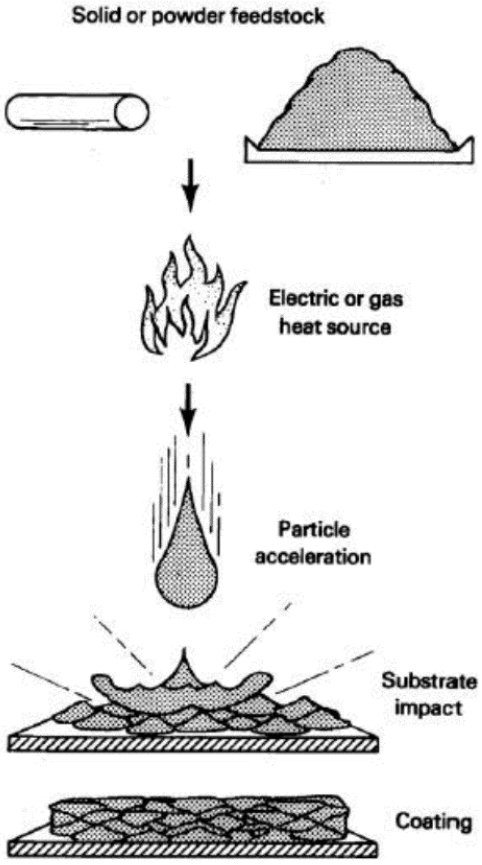

Figure 2-1. Thermal spraying deposition process [8].

Plasma spray [9], high velocity oxygen fuel (HVOF) [10], wire arc spray, and cold spray are among the commercially attractive thermal spraying techniques. Vacuum plasma spray produces superior coatings and is utilized in production of aircrafts and jet engine components

[11]. This is a costly method since it requires a vacuum condition during the deposition process. Among various deposition techniques, wire arc spray and cold spray have some advantages that are further discussed in the next sections.

Figure 2-2 shows various thermal spraying methods in terms of generated gas temperature and particle velocity during the deposition process.

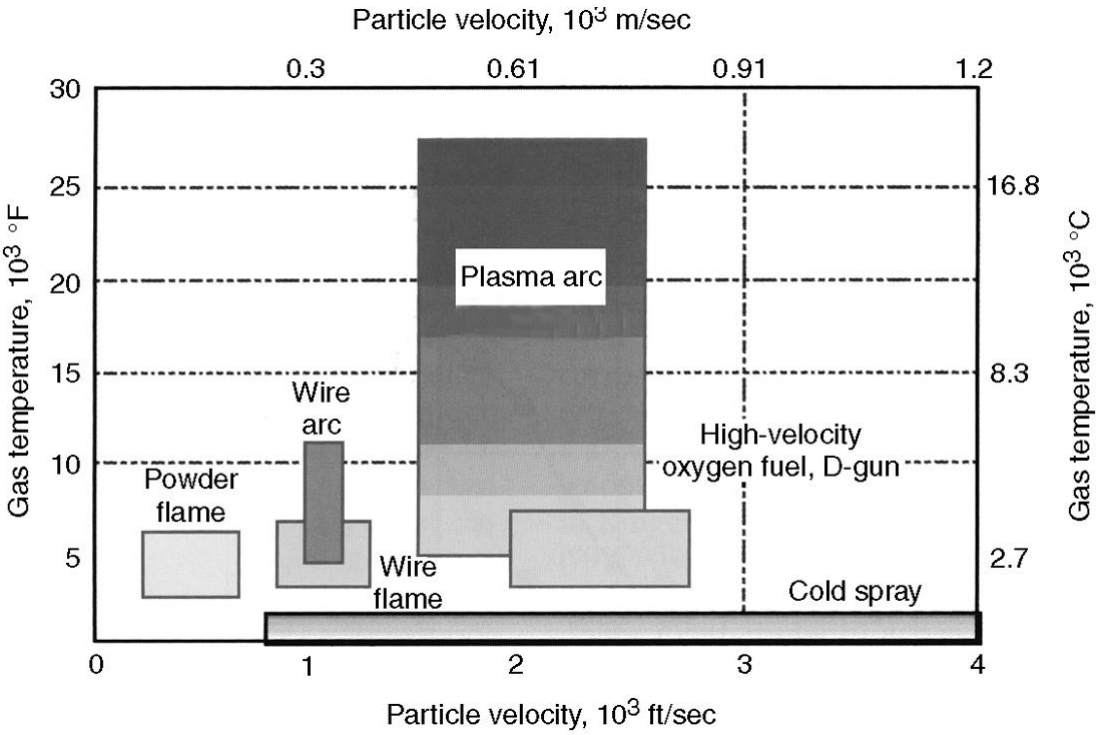

Figure 2-2. Gas temperature vs particle velocity for common thermal spray techniques [8].

2.3.1. Wire Arc Spraying

Wire arc spray uses electrical energy to produce an electric arc between tips of the two wires made from desired coating materials, which are continuously fed to the system. The tips of the wires melt instantly due to the local high temperature produced by the strong arc and a pressurized gas accelerates molten droplets toward the substrate. Since the molten particles are carried by an air stream instead of a hot jet of gas, the heat input and consequently the temperature of the substrate does not increase drastically. The advantage of this process is the low cost, ease of

use, and high deposition rate compared to other techniques [8]. However, due to thermal stresses that are built up due to melting and re-solidification of the particles, thickness of the deposited coatings is limited. On the other hand, the materials that can be deposited through this technique are only limited to those that can be formed into a wire and conductive. To this end, it can only be used for spraying metallic materials. Schematic of a wire arc deposition process is shown in Figure 2-3 [12]. Commercially available wires of aluminum and zinc can be used to deposited protective layers with wire arc deposition method for corrosion protection of industrial components.

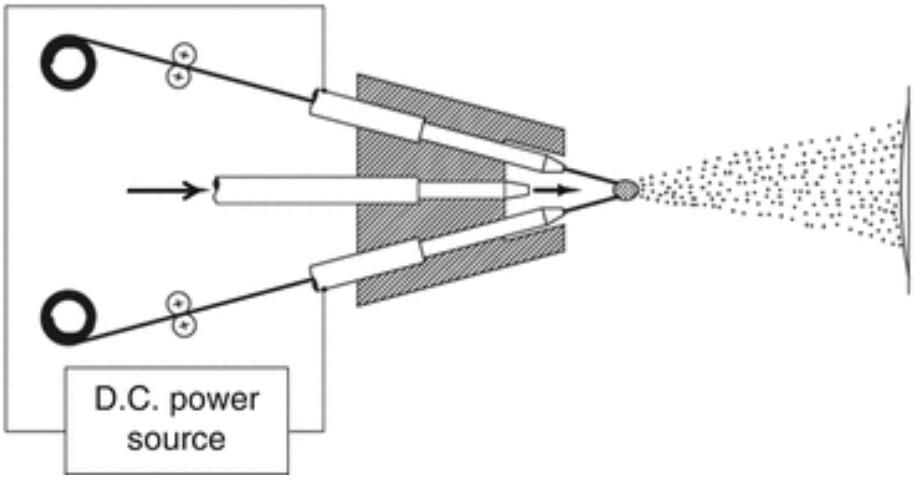

Figure 2-3. Schematic of wire arc deposition technique [12].

2.3.2. Cold Spraying

The term “cold spraying’ comes from the fact that powders of the coating material are deposited on the substrate without melting. The deposition temperature is in the range of 0 to 700 °C, which is generally lower than the melting range of coating particle materials. This method utilizes highly pressurized gas with a velocity that ranges between 300 to 1200 m/s to carry the solid particles towards the substrate. The high velocity causes the solid-state particles to deform and make a mechanical bond with the surface. Production of thick coatings is possible through the cold spray deposition technique because there are no thermal stresses built in the coating during

spraying process. Since the deposition is mainly dependent on the deformation of solid particles, cold spray technique is applicable for ductile materials only. Nevertheless, brittle of hard materials can be co-deposited with a ductile matrix material [8]. High ductility of aluminum and zinc powders makes them ideal materials to be deposited by the cold spray technique.

In general, mechanical properties of the coatings fabricated by thermal-spray coatings are mainly based on their microstructure characteristics and interfacial properties between splats. For a majority of thermal spraying techniques, which involve melting of the materials during deposition and solidification processes, impact of molten particles to the surface form an interlocked lamella structures between the splats. The grains grow across the thickness of the splats and often oriented in the direction of the temperature gradient [13]. The ideal geometry for splats are round or pancake shape, which can produce more uniform structures [14].

During deposition process, undesirable phases including oxides, pores and voids may form and affect the microstructure of the coatings [15]. Therefore, appropriate characterization of coating materials will significantly improve our understanding of critical microstructural features that affect the physical and mechanical properties of the coating structures. It is essential to develop an efficient microstructural-based scheme to evaluate the mechanical properties of thermal sprayed coatings. There is a significant difference between the properties of as-sprayed deposits and conventionally processed materials.

CHAPTER 3. INVESTIGATION ON RELATIONSHIP BETWEEN MICROSTRUCTURAL CHARACTERISTICS AND MECHANICAL PROPERTIES OF WIRE ARC SPRAYED ZN-AL COATING[1]

3.1. Abstract

Wire arc spraying is a cost-effective thermal spraying technology to deposit a protective coating layer on the surface of industrial components. Mechanical properties of wire arc spraying coatings are mainly influenced by their heterogeneous microstructure, resulting in complex and anisotropic mechanical properties. The objective of this investigation is to characterize the mechanical behavior of wire arc sprayed Zn-15Al alloy using an efficient micromechanical-computational scheme. The SEM micrographs were imported to an object-oriented finite element scheme and distinguished into various phases, such as voids and cracks, then subsequently discretized into finite elements. To examine the validity of this technique, experimental studies, such as Knoop and Vickers microhardness, resonance frequency, and nanoindentation, were conducted on the free-standing coating samples. The elastic modulus of the coating was also calculated using well-known analytical methods. Comparison of the results obtained in this study was used to investigate the relationship between the microstructural features and mechanical properties in coating materials. Image-based FEA showed good agreement with the experimental measurements and proved the effect of splat boundaries on the reduction of mechanical strength

[1] The material in this chapter is co-authored by Amir Darabi and Dr. Fardad Azarmi. Amir Darabi wrote this chapter in consultation with Dr. Fardad Azarmi. This chapter is submitted for publication.

between coating layers and consequently, lower elastic modulus of the wire arc sprayed Zn-15Al coating in the longitudinal direction compared to the transversal one.

3.2. Introduction

Thermal spraying is an advantageous method for depositing protective layers on the surface of parts, components, and structures. Coatings deposited by thermal spraying techniques have found many applications in aerospace, automotive, biomedical, electrical, and turbine industries [7]. Wire arc spraying is a member of thermal spraying family that has found extensive commercial use thanks to its low cost, ease of use, and relatively high deposition rate compared to other thermal spraying techniques [8]. Metals with good corrosion resistance such as zinc and aluminum [16-18] could be deposited via wire arc deposition or flame spray techniques to improve the anti-corrosion properties of industrial components; this process is known by the industry as "Metallization" [19-21]. Recently, it has become popular in the pipeline industry and is commonly used to protect metallic pipes and structures against environmental damages such as corrosion and erosion [22]. Fayomi *et. al* [23] have shown that zinc-based aluminum alloys exhibit better corrosion resistance compared to the pure zinc or aluminum materials. The mechanical and tribological behavior of zinc-aluminum alloys have made them one of the most favored materials for corrosion resistant coatings in various industrial applications.

Wire arc spraying uses electrical energy to produce an arc between the two wires made from desired coating materials, which are continuously fed to the system. The tips of the wires melt immediately due to the high temperature produced by the strong arc, and pressurized gas accelerates molten droplets toward the substrate [12]. These molten particles are solidified, and the coating is formed by the accumulation of incoming particles layer-by-layer. During this process, because of thermal stress build-up during impact and solidification processes, the coating

structure undergoes notable changes in terms of mechanical properties. In addition, the formation of unwanted phases considerably alters the mechanical behavior of the coating. Therefore, the mechanical properties of thermal spray coatings are highly dependent on microstructural features [24]. Some studies have investigated the relationship between the microstructure and mechanical behavior of thermal spray coatings [25-28]. These studies have only taken into account the volume fraction of unwanted phases in the microstructure It is worth mentioning that the volume of unwanted phases as well as the location and distribution of them over the microstructure can significantly affect the behavior of thermal spray deposits. Therefore, some studies have proposed investigating the influence of the microstructural features by studying actual images taken from the coating microstructure [29, 30].

This study aims to extend the understanding of microstructural characteristics and their effect, by conducting image-based analysis on wire arc "metallization" deposited coatings. In addition, mechanical experiments along with analytical methods were performed to evaluate the results obtained from numerical simulation. To this end, SEM images taken from random locations across the cross-sectioned of wire arc sprayed Zn-Al coating were subjected to Object-Oriented Finite (OOF) element to measure the elasticity of the coating. Furthermore, theoretical models proposed for inhomogeneous and porous structures were applied to calculate the mechanical properties of the coating. Finally, mechanical tests such as Resonance Frequency Analysis (RFA), nanoindentation, and microhardness tests such as Knoop and Vickers indentation were conducted to validate the elastic modulus measurements performed by OOF.

3.3. Experimental Procedure

3.3.1. Coating Deposition and Sample Preparation

Wire arc spraying technique is employed to deposit Zn-15Al coating samples. Commercially available wires of zinc alloys containing 15% aluminum (Oerlikon Metco, Westbury, NY, USA) with a density of 7.18 g/cm3 were fed parallel into a ValuArc 200 Electric wire arc spray gun (Oerlikon Metco, Westbury, NY, USA). A coating with 1 mm thickness was deposited on an aluminum substrate. The spraying parameters are listed in Table 3-1.

Table 3-1. Spraying parameters used for wire arc deposition.

Process Parameters	**Value**
Spray Distance	180 mm
Wire Feed rate	28m/min
Voltage	30 (V)
Pressurize Gas	Air

3.3.2. Microstructural Characterization

First, the coating sample was sectioned and mounted in epoxy (Buehler transoptic powder). Next, the sample was subjected to grinding up to 1200 grit and polishing using 3-micron diamond suspension on Spec-Cloth to be suitable for metallography.

3.3.2.1. Scanning Electron Microscopy

A JEOL JSM-6490LV SEM (JEOL, Peabody MA, USA) was used to perform Scanning Electron Microscopy (SEM) on the sample to have a better perception of the distribution of pores and splat boundaries. Micrographs were taken at a voltage of 15 keV. In addition, a nano-trace Energy-Dispersive X-ray Spectroscopy (EDS) detector from thermos-scientific, Madison, WI, USA was used for elemental analysis on the microstructure.

3.3.2.2. Image Analysis

SEM micrographs taken from random locations in the coating microstructure were subjected to image analysis to calculate the porosity level of the coating samples. Seven different micrographs were studied by iSolution DT software (iMTechnology Co.) according to ASTM E1245 and E562 [31, 32].

3.3.3. Mechanical Tests

3.3.3.1. Knoop Indentation

Indentation techniques are commonly used to measure the resistance of thermal spray coatings to deformation under certain applied loads [33]. Knoop and Vickers indentation methods are the most favorite methods of hardness measurement and they are both used in this study. The main feature of Knoop indention method is the wide area covered by the elongated diamond shape of the indenter. The wider geometry of the indenter helps to cover more microstructural features such as pores and splat boundaries to be included in each indent. As a result, overall characteristics of the wire arc sprayed coating can be observed using this method in two directions, longitudinal (parallel to spray direction) and transversal (parallel to the substrate surface) as shown in Figure 3-1 [34]. Knoop indentation was conducted using a Clark CM-800 AT microhardness tester under an applied load of 1 kgf and a dwell time of 15 sec. The value is reported in terms of HK, obtained from Eq. 2-1. This test was repeated nine times to achieve better accuracy.

$$HK = 14.229 \times \frac{F}{d_K^2} \tag{3-1}$$

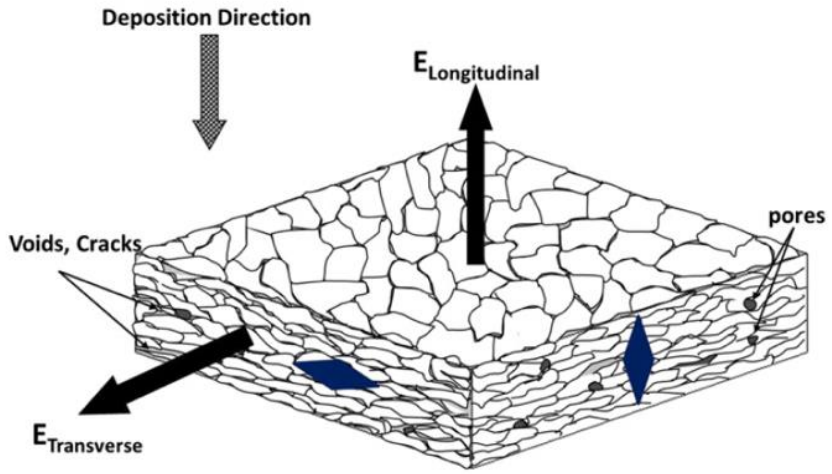

Figure 3-1. Knoop indentation in longitudinal and transversal directions [34].

3.3.3.2. Vickers Indentation

To validate the results from Knoop indentation, Vickers indention was performed on the samples using the same microhardness tester by replacing Knoop indenter with a Vickers one. Each hardness test was applied under1kg load for 15 sec. Since the Vickers indenter is square shaped, there was no need to perform the indentation in multiple directions. Fifteen Vickers indentation were conducted on the cross-section of the coating sample with respect to ASTM E92-17.

3.3.3.3. Nanoindentation

Compared to Knoop and Vickers microhardness tests, the size of indentation is small enough that each of them may locate on a single phase or feature in the coating microstructure [35]. Wire arc sprayed Zn-Al coating sample was subjected to nanoindentation test in which three loading stages were applied. Initially, the load is increased to a specific value, then it is kept constant for a certain time, and finally, it decreases to zero. In this study, a Tribo-Indenter 900 form Hysteron Inc. USA, was used in a quasi-static mode to make a total of sixty indentations in transversal and longitudinal directions. Due to the nano scale size of the indenter, multiple

indentations needed to be applied in each direction to make sure that all features within the microstructure were examined by indenter during the test. In the case of coating microstructure, the large number of indentations increases the possibility of gathering hardness information of each phase such as splats, splat boundaries, and voids. The average hardness values obtained from multiple indentations represent the overall hardness of the coating sample.

3.3.3.4. Resonance Frequency Analysis

Impulsive Excitation, also known as Resonance Frequency Analysis (RFA), is an accurate and non-destructive method of measuring important mechanical properties of a specimen at various temperatures. In this technique, a hammer continuously excites (taps) on one side of the sample, and the vibrations are detected by a microphone on the other side. A software package analyzes these vibration signals and determines the mechanical properties of the sample such as elastic modulus, shear modulus, and Poisson ratio. This technique is of significant accuracy and is used as a validation source for results obtained from other experimental measurements. To prepare the samples for RFA, coating and substrate were separated, and the coating was sectioned into a bar with the size of 40 mm × 5 mm × 1.5 mm. Free standing coating specimen was slightly grinded and polished for more accurate measurements prior to RFA. A Resonance Frequency Analyzer from IMCE, Belgium was employed in this study and results are reported based on the average of five repetitions of the test.

3.4. Results and Discussion

3.4.1. Microstructural Characterization

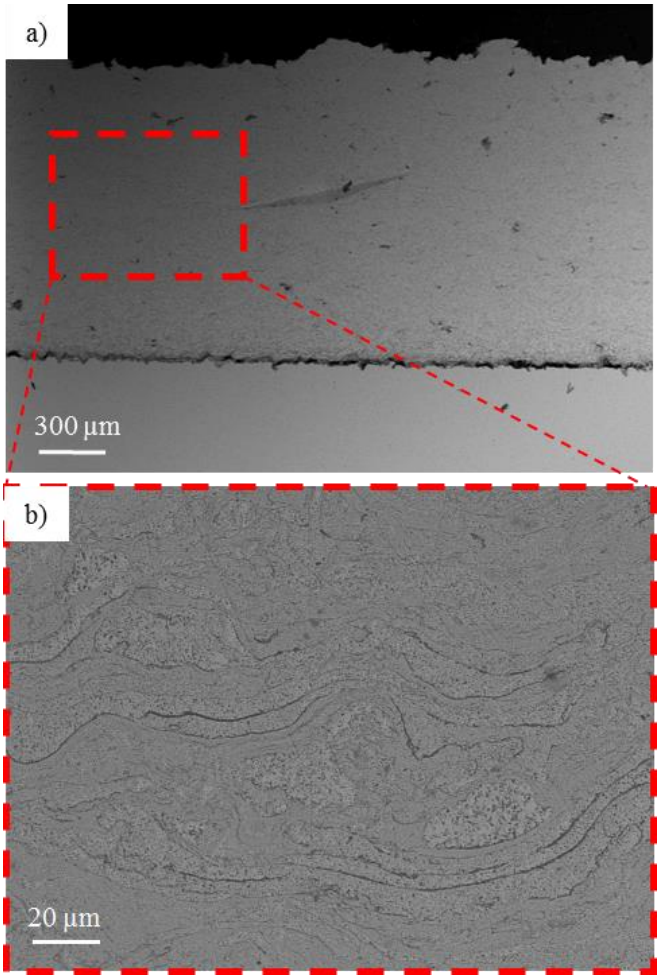

Figure 3-2. SEM image from the cross-section of the wire arc sprayed Zn-15Al coating at a) low and b) high magnifications.

Figure 3-2 (a) shows a low magnification SEM micrograph of the coating and substrate cross-section. Only porosity distribution within coating microstructure can be seen in those low magnification micrographs. More details of coating microstructural features and splat boundaries can be detected over the higher magnification micrograph shown in Figure 3-2 (b). The microstructure mainly includes gray and dark regions. Dark area represents porosity and splat boundaries. EDS analysis was performed nine times on random locations on the gray region and

the results indicated that the coating material was an alloy consisted of a mixture of 18.21±2.02 wt.% aluminum and 81.78±2.02 wt.% zinc. These results are in fair agreement with the nominal composition of the feedstock wire of Zn-15Al used in this study.

Figure 3-3 (a) shows an SEM micrograph of the coating sample in this study. Splat boundaries and pores were detected by the software and were assigned by blue color pixels for better identification (Figure 3-3 (b)). A porosity of 7.35 ± 0.93% was obtained for the coating samples deposited in this study.

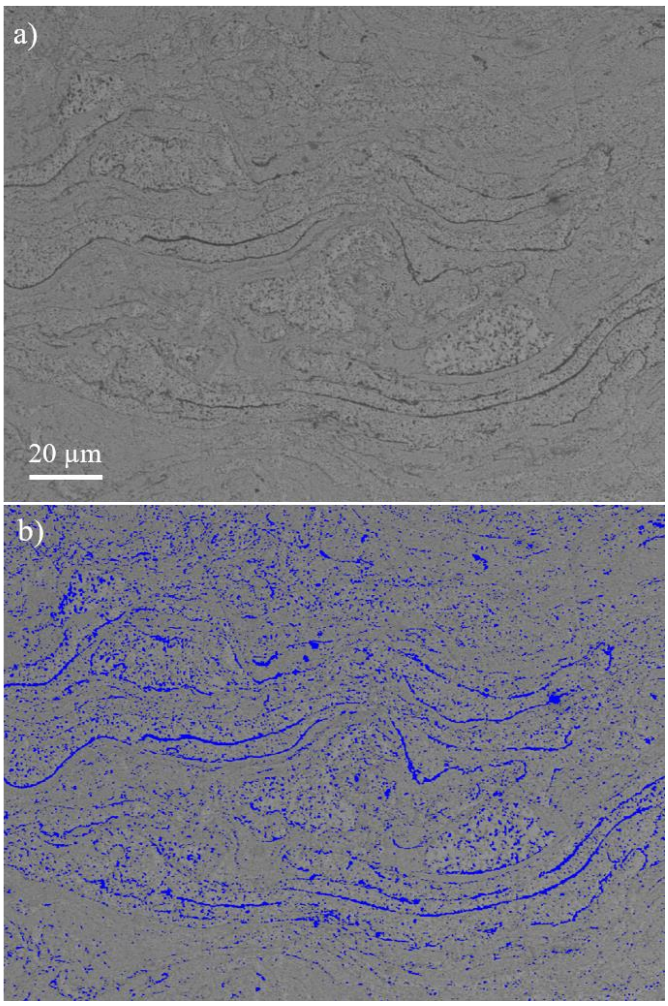

Figure 3-3. a) SEM micrograph of the wire arc deposited Zn-15 Al and b) the location of pores, voids, and splat boundaries obtained by image analysis.

3.4.2. Mechanical Tests

3.4.2.1. Knoop Indentation

Figure 3-4 shows a Knoop indent on cross-section of the Al-15Zn coating sample. There are no signs of crack around the edges of the indentation, which indicates the ductility of the coating material after the thermal spraying process. The results obtained from nine Knoop measurements in both transversal and longitudinal directions are shown in Table 3-2.

An analytical method developed by Marshall *et al*. is capable to estimate elastic modulus using hardness values obtained from Knoop test [36] as shown in Eq. 2-2.

$$E = \frac{\alpha_1 HK}{\frac{b}{a} - \frac{b'}{a'}}, \tag{3-2}$$

where b and b' are half of the short diagonal of the indenter and the indent, and a and a' are half of the long diagonal of the indenter and the indent, respectively. α_1 is a constant that is suggested to be equal to 0.34 by Meredith *et al*. [37].

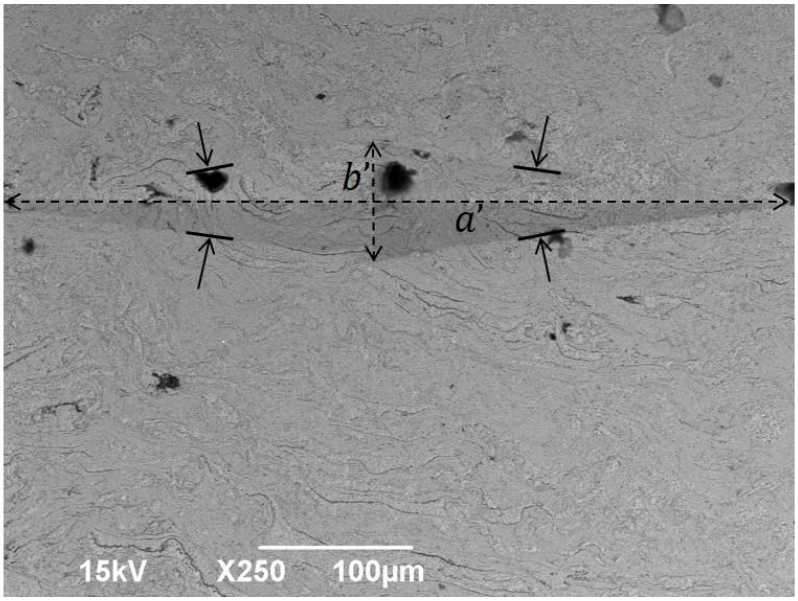

Figure 3-4. Major and minor diagonals of a Knoop indent.

The values of a' and b' are measured after each indentation, while the ratio of b to a can be calculated according to ASTM E92-17 (Eq. 2-3). As suggested in this standard, the edge angle of a Knoop indenter is 172.5°. The corresponding elastic moduli were calculated using Marshall's equation (Eq. 2-2) and the results are illustrated in Figure 3-5. As expected, the hardness was slightly higher in transversal direction due to the presence of fewer splat boundaries that are weakening regions in the microstructure of the coating.

$$\frac{b}{a} = \frac{\tan(\frac{172.5^o}{2})}{\tan(\frac{130^o}{2})} = \frac{1}{7.1144} \tag{3-3}$$

Table 3-2. Knoop indentation results on Zn-15Al wire arc sprayed coating.

Zn-15Al	**Hardness (HK)**	**Elastic Modulus (GPa)**
Transversal	46.83 ± 1.94	16.85 ± 2.99
Longitudinal	44.83 ± 0.97	13.43 ± 2.37

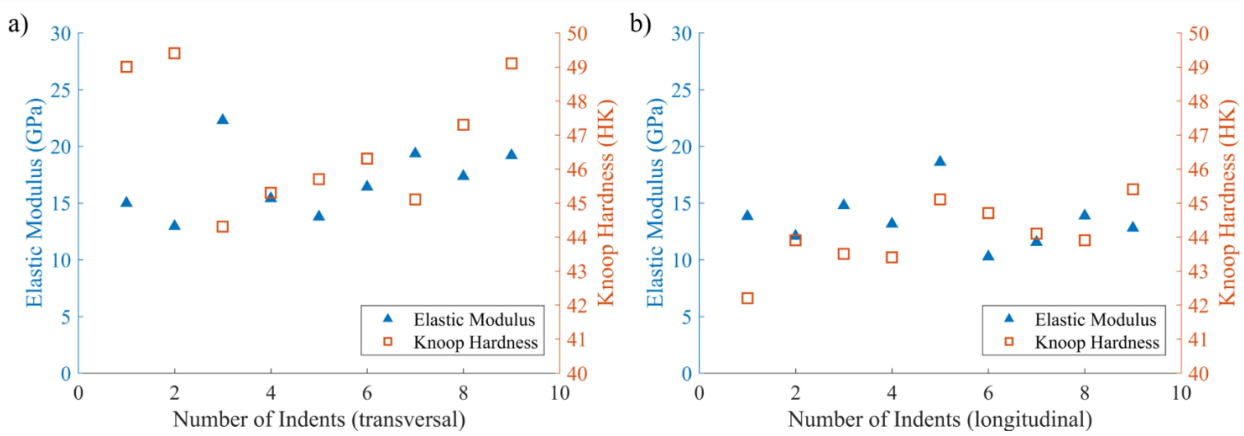

Figure 3-5. Knoop hardness measurements and corresponding elastic moduli in a) longitudinal, and b) transversal directions.

3.4.2.2. Vickers Indentation

The hardness of the coating material was measured again using Vickers indentation to validate the ones obtained from Knoop indentation test. An average hardness value of 45.29 ± 1.70 HV was obtained from the fifteen Vickers indentations. Both experiments showed nearly the same

results for the hardness of wire arc sprayed Zn-15Al. However, compared to the rule of mixture, taking to the account the nominal hardness of zinc and aluminum, the coating exhibits much lower hardness value. In addition, according to the literature, the measured values for extruded and annealed alloys of Zn-15Al were 60 HV and 80 HV, respectively [38]. The lower hardness values obtained for Zn-15Al wire arc sprayed coating could attribute to the existence of porosities, splat boundaries, and thermal stress build-up during the deposition process, which can greatly reduce the hardness of the coating [39].

3.4.2.3. Nanoindentation

Figure 3-6 shows load vs displacement obtained from the results of thirty indents made on the surface of the Al-15Zn coating cross-section in both transverse and longitudinal directions. A curve of average value was fitted along those data as shown in Figure 3-6, for longitudinal and transversal directions. The nano-hardness results obtained in both directions have almost similar values of 0.88 ± 0.24 GPa and 0.87 ± 0.33 GPa in transversal and longitudinal directions, respectively. Nanoindentation also reports reduced modulus that is a combination of elastic deformation in the indenter and the coating sample [40]. Since nanoindentation measures the reduced modulus of the coating, Eq. 2-4, proposed by Dejun *et al*. [41], is used to convert them to elastic modulus.

$$E = \frac{1-\nu^2}{\frac{1}{E_r} - \frac{1-\nu_i^2}{E_i}} \tag{3-4}$$

E and ν are Young's modulus and Poisson ratio of the coating sample and E_r is reduced modulus. The elastic constants of the diamond indenter are suggested as $E_i = 1141$ GPa and $\nu_i = 0.07$.

The calculated elastic moduli were 87.58 ± 13.07 GPa in transversal, and 71.07 ± 16.41 GPa in longitudinal direction. The high standard deviation in the nanoindentation experiment

results is correlated to the nano scale measurements of the mechanical properties of the different microstructural features in this experiment. Nano size indenter could land on the coating material with higher strength or on voids with very low values of mechanical properties. Results from nanoindentation test indicated that the coating exhibited higher strength in transversal direction compared to the longitudinal one.

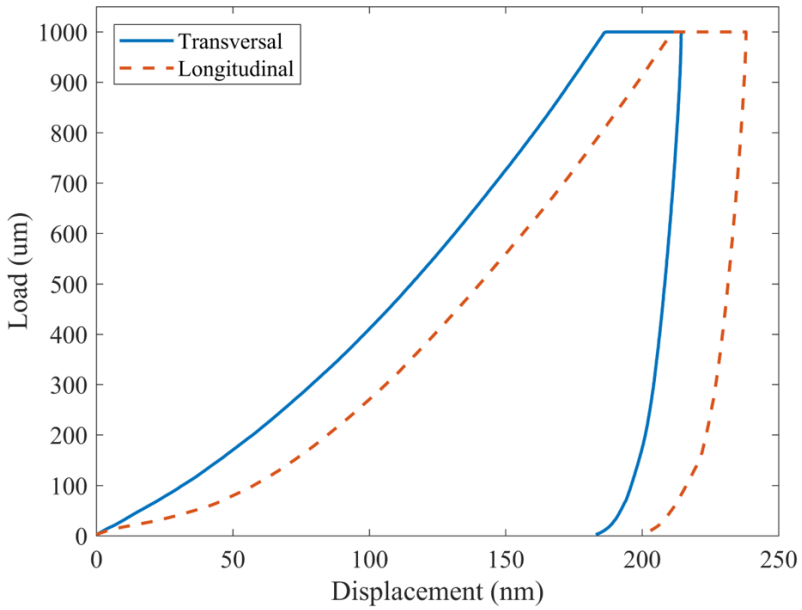

Figure 3-6. Load vs. Displacement curve obtained from nanoindentation.

3.4.2.4. Resonance Frequency Analysis

RFA is the most accurate mechanical experiment among other methods used in this study. However, RFA is only capable of measuring the material behavior in the transversal direction, due to the nature of this experiment. The measured elastic modulus, shear modulus, and Poisson ratio were 51.27 ± 0.01 GPa, 19.62 ± 0.02 GPa, and 0.306 ± 0.001. The small amount of standard deviation is an indicator of the high accuracy of this analysis. Accordingly, RFA was considered as a reference to validate the results of other methods. By comparing the obtained values with the literature, where the elastic modulus for Zn-15Al wire used for thermal spraying is reported

between 70 GPa and 90 GPa [42], the Zn-15Al wire arc sprayed coating exhibited lower elastic modulus. This decrease could be correlated to the existence of porosities and splat boundaries in the coating microstructure.

3.5. Numerical Analysis

Finite Element Analysis (FEA) is a desirable method to estimate properties of the materials using numerical simulation without performing actual mechanical experiments. However, it is essential to have accurate information regarding the various features and characteristics of the material under investigation. There are various FEA packages available for examination of the properties of homogeneous materials. In the case of thermal spray coatings, since the coating exhibit an inhomogeneous microstructure, those commercially available FEA are not capable of providing an accurate estimation of the properties. To this end, access to an FEA scheme with the ability to use real microstructural images of the material under investigation is crucial for obtaining accurate results. Object-Oriented Finite (OOF) element developed by the US National Institute of Standards and Technology (NIST), estimates materials behavior using actual micrographs taken from the material. This image-based numerical analysis is much more reliable compared to other FEA packages in this study due to its ability to take into account pores, voids, and splat boundaries and their distribution, using high quality SEM micrographs, leading to a comprehensive evaluation of mechanical properties of the coating materials. However, the challenge is to find the optimized magnification that cover a large area of the microstructure to include sufficient microstructural features which can be a representation of the coating microstructure. On the other hand, it is difficult to visibly identify small microstructural features in low magnification micrographs which represents a large area of the microstructure. It means that selected images must be taken at high enough magnification to show small areas with all existing features. To this end, several SEM

micrographs were examined to select the optimum magnification. The same methodology as described by Azarmi *et al.* [43] was employed to define the optimum magnification. Different contrasts in micrographs taken at different magnifications were assigned properties and discretized to small elements at different sizes. The optimum processed (meshed) micrograph was the one which had more similar features as original micrograph with minimum elimination of microstructural features.

Three SEM images taken randomly from the cross-section of Zn-15 Al coating sample with the optimum magnification were subjected to OOF in this study. It is important to capture images that represent an acceptable section of the coating cross section that sufficiently includes maximum number of the microstructural features. Each image includes thousands of pixels that were divided into different groups based on their contrast. With the assumption of a contrast threshold, pixels can be divided such that those above the threshold are considered as the matrix, while others are belonged to the pores group. Finding the optimum threshold is another challenge in this numerical simulation. Since the porosity percentage can be obtained by the ratio of pixels to the total number of the pixels, the threshold should be optimized with respect to the porosity measurement performed using image analysis software. Three threshold values were used to find the average porosity using three different SEM micrographs of the coating microstructure. Figure 3-7 shows that the second assumption for the threshold resulted in an area fraction of 8.86 ± 1.05 %, which is the closest value to the porosity measurement by image analysis.

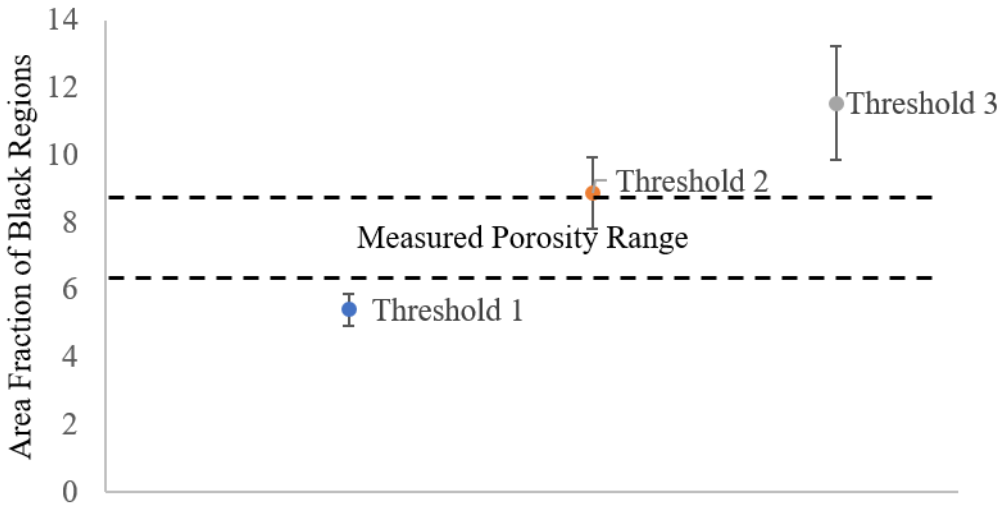

Figure 3-7. Comparison of three contrast thresholds with respect to the coating porosity.

Two different sets of contrast were created on the microstructure using the second assumption for the threshold value to better distinguish the phases in the coating microstructure. Therefore, all the contrasts above the threshold are shown in gray, representing the coating material Zn-15Al, while those below the threshold are shown in black, representing the pores, voids, and splat boundaries. Figure 3-8 (a and b) show SEM micrographs and the resulting processed image.

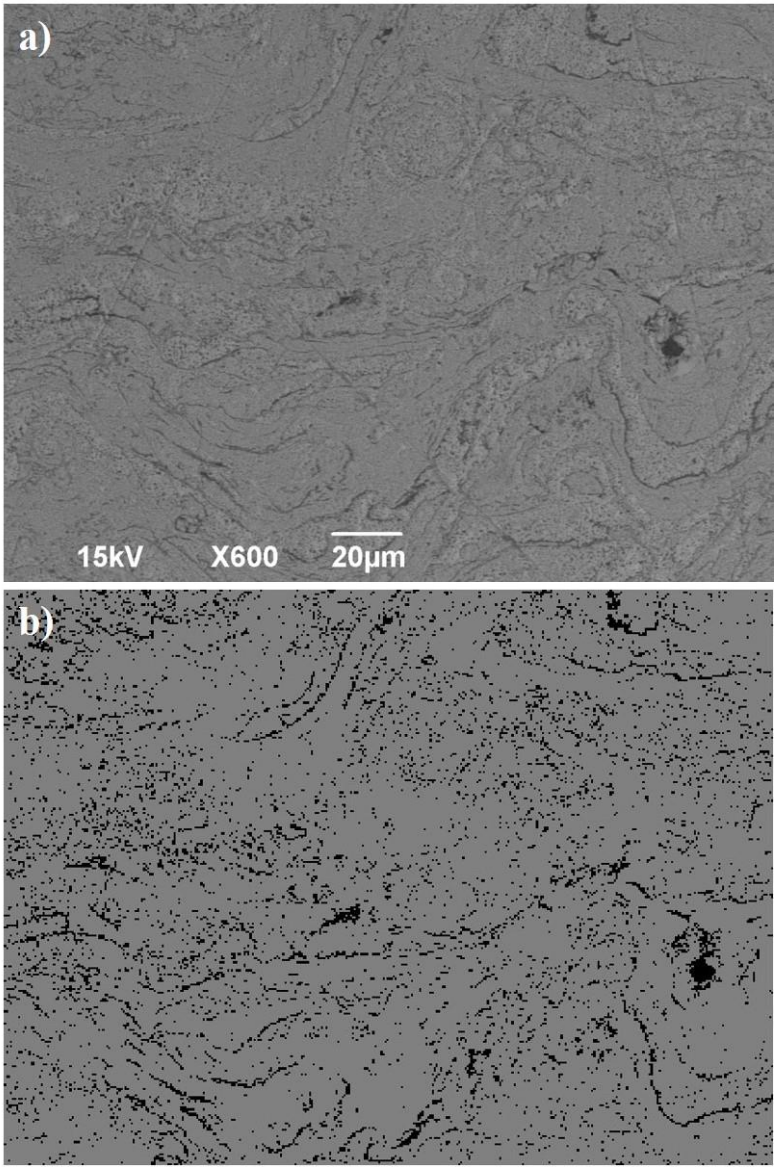

Figure 3-8. (a) SEM micrographs of the coating sample, and (b) processed image using OOF.

Consequently, each set of pixels were assigned a value for elastic modulus and Poisson ratio as shown in Table 3-3.

Table 3-3. Material properties assigned to different pixels in OOF.

Material	**Elastic Modulus (GPa)**	**Poisson Ratio**
Zn-15Al	93.1	0.26
Pores and Voids	E-9*	0.26

The mechanical properties of Zn-15Al were calculated using the rule of mixture (Eq. 2-5). As for pores and voids, the elastic modulus was set to a very small amount, and an equal Poisson ratio as of Zn-15Al was assigned to the pore pixels.

$$\log E_0 = \nu \log E_{Al} + (1-\nu) \log E_{Zn} \tag{3-5}$$

where v is the volume fraction of aluminum, while E_{Al} and E_{Zn} are the elastic modulus of aluminum (70 GPa) and zinc (100 GPa), respectively. The values were obtained from the CES Edupack database [42]. In addition, specific colors were assigned to both groups for better differentiate visible regions in the microstructure. Figure 3-8 (a and b) show SEM micrographs and the resulting processed image. It is worth mentioning that all dark regions in Figure 3-8 (a) were assigned as porosity. In fact, this is not a correct assumption, since some of those regions could appear darker due to the angle of tilt inside SEM or small differences in composition at splat boundaries. It could affect the accuracy of the calculation in this technique. The importance of finding optimum magnification in this regard to better distinguish different microstructural features is a key point here [43].

The next step is creating a structure of elements named skeleton, which can be modified to increase homogeneity in the selected elements. Figure 3-9 shows step-by-step modifications made on the skeleton using available tools in the software. The final skeleton reached a homogeneity level of approximately 97%. The final mesh is generated based on the skeleton created in this step. Subsequently, boundary conditions were carefully chosen to avoid the material yielding. Finally, the program solves a "Force Balance" problem and analyzes the average stress and strain over the micrograph of the coating. The elastic modulus of the coating sample is calculated using Eq. 2-6 for plane stress condition since the analysis is based on a 2D image [44].

$$E = \frac{\sigma_{xx}(1-\nu)}{\varepsilon_{xx}} \tag{3-6}$$

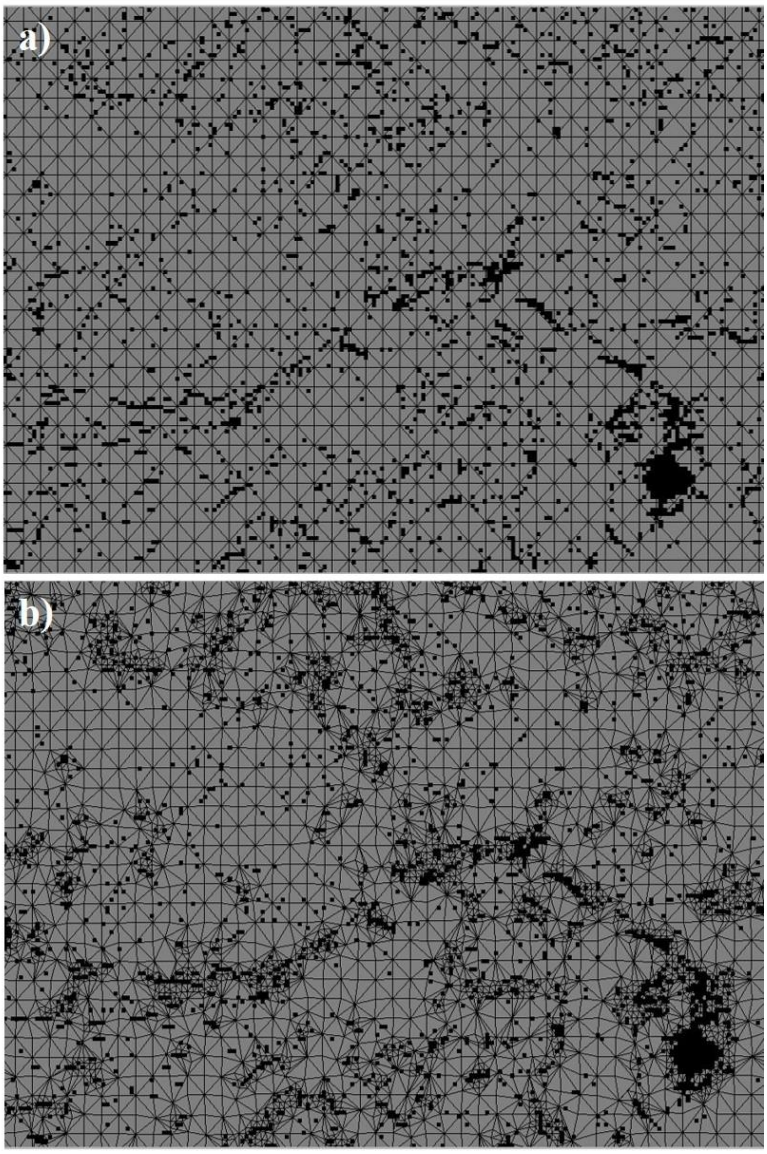

Figure 3-9. Skeleton modification process performed by OOF, a) original skeleton, b) annealed and modified elements.

The analyses showed an elastic modulus of 56.18 ± 1.04 and 53.01 ± 0.88 GPa in transversal and longitudinal directions, respectively. FEA analysis predicted higher elastic modulus in the transversal direction and this outcome is in agreement with the results obtained by

experimental procedures. The final mesh and the stress distribution over the micrograph of the wire arc sprayed Zn-15Al coating is shown in Figure 3-10.

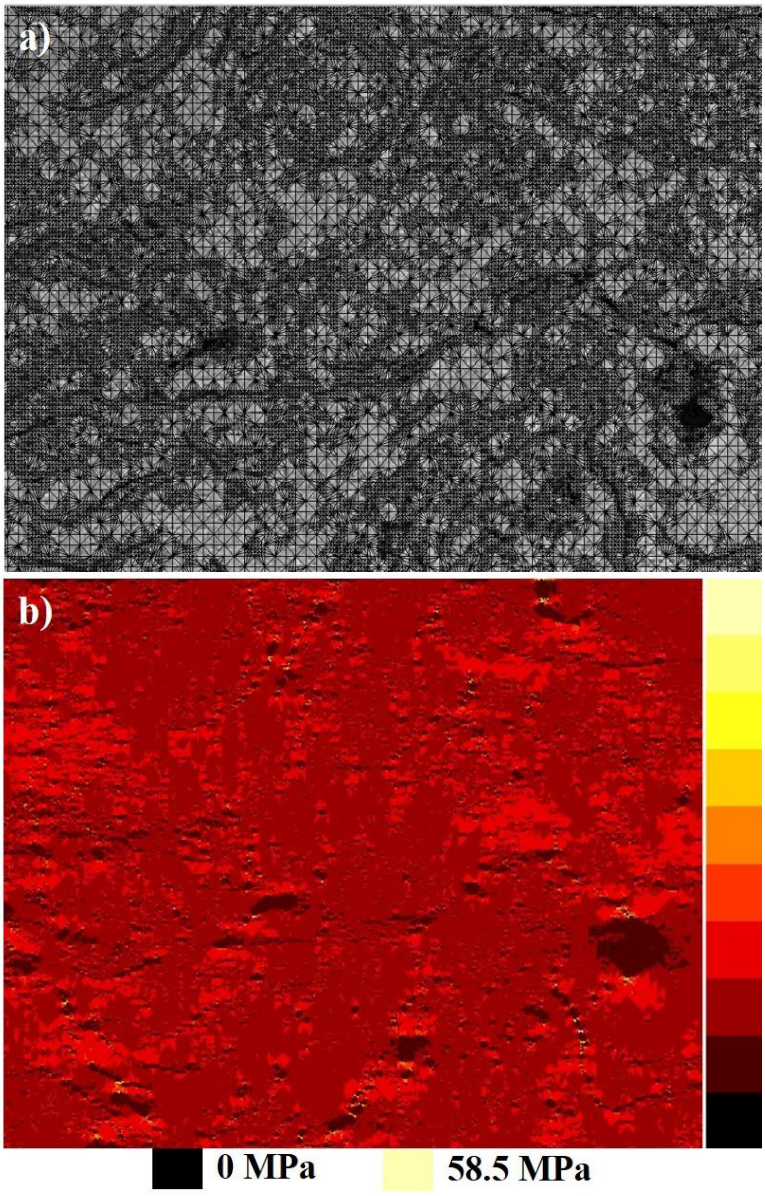

Figure 3-10. a) Final meshed structure by OOF, and b) stress distribution map over the micrograph.

3.6. Analytical Model

Several analytical methods have also been developed to relate the mechanical properties to the microstructural characteristics of materials. Based on the microstructure of coatings in this

study, two different available analytical models are utilized in this study to evaluate the mechanical behavior of the wire arc sprayed coatings in this study to better validate previous results. The model developed by Hashin-Hasselman [45] has taken into account the porosity of the coating. This model measures the elastic modulus of materials purely based on the level of porosity that exists in their microstructure.

$$E = E_0\left[1+\frac{Ap}{1-(A+1)\,p}\right], \tag{3-7}$$

where E_0 is the nominal elastic modulus of the bulk material, A is a constant equal to -33.4, and p is the porosity level. It is assumed that Zn-Al mixed to form a composite material and to this end, the rule of mixture is employed to calculate nominal elastic modulus E_0 of Zn-15Al alloy (Eq. 2-5). In addition, the porosity of the coating was measured using image analysis. The elastic modulus was calculated as 25.51 GPa. The analytical model proposed by Hashin-Hasselman underestimates the elastic modulus of the coating by a large amount.

To better differentiate the results obtained from experimental methods, numerical simulations, and analytical models, Table 3-4 shows all the measured elastic moduli for the wire arc sprayed Zn-15Al coating sample.

Table 3-4. The comparison of the results of elastic modulus measurement from various methods in this study.

Method	**$E_{Transversal}$ (GPa)**	**$E_{Longitudinal}$ (GPa)**
RFA	51.27 ± 0.01	-
Nanoindentation	87.58 ± 13.07	71.07 ± 16.41
OOF	56.18 ± 1.04	53.01 ± 0.88
Marshall equation	16.85 ± 2.99	14.01 ± 3.93
Hashin-Hasselman	25.51	-

As mentioned before, RFA is considered as the most accurate measurement technique of mechanical properties and the value obtained from RFA can be considered as a reference to

evaluate the accuracy of all characterization methods in this study. It is obvious that Marshall model, which is mostly based on the geometry of the Knoop indent, was not successful to accurately predict mechanical properties of Zn-15 Al coating in this study. This model is very sensitive to the measurement of the major and minor diagonal length of the Knoop indent by the operator. The slightest error in measurements may result in an imprecise calculation of elastic modulus. On the other hand, nanoindentation could not equally take to the account information from indents landed randomly on different features in the coating microstructure of the wire arc sprayed coating. Apparently, a small number of indentations were made on pores and splat boundaries, while most of them are solely made on the coating material, resulted in obtaining higher than acceptable value for elastic modulus.

The large standard deviation in the results obtained from nanoindentation also proves inconsistency of the results. Regardless of obtained values for mechanical properties, load vs, displacement curves obtained from nanoindentation showed less displacement, indicating higher strength in transverse direction compared to longitudinal one and showing an agreement with other results from different techniques applied in this study. The higher strength in transverse direction compared to the longitudinal one could be because of the existence of more splat boundaries in the longitudinal direction due to spraying direction. From a total of thirty nanoindents in each direction, the calculated elastic modulus is more than 15% higher in the transversal direction, and since the nanoindents could land on single phases or features due to its small size, these results could correlate to the higher number of indents landed on splat boundaries in the longitudinal direction. This fact can also be concluded from other techniques used in this study, which showed a higher elastic modulus in transversal direction. Considering the nature of thermal spraying

methods, due to the layer-by-layer accumulation of the coating, the elasticity of the coating will be lower in longitudinal direction because of the effect of splat boundaries.

Hashin-Hasselman model estimated much lower elastic modulus that indicates the inaccuracy of this analytical model. There are a couple of reasons for inaccuracy in this model, first, the elastic modulus of the alloy Zn-15Al is calculated using the rule of mixture and may not reflect the actual elasticity of the material. Second, the model just considered the amount of porosity and neglected the effect of their location and distribution over the microstructure.

Image-based FEA analysis in this study was able to estimate the elastic modulus of the coating within an acceptable range. It could be due to taking into account all the microstructural features using SEM images at high resolution. OOF was capable of evaluating the mechanical properties of the coating. The small deviation from actual values could be due to the fact that image-based numerical simulation is applied on a 2D scheme developed from the microstructural image that may not be an accurate reflection of a 3D characteristic of the materials.

3.7. Conclusion

The aim of this study was to investigate the effect of microstructural features on the mechanical behavior of thermal spray coatings. Different experimental techniques were employed to find the mechanical properties of wire arc sprayed Zn-15Al coating. In addition, image-based finite element analysis was used to find the elastic modulus of the coating with respect to actual high-quality SEM images of the coating microstructure. RFA was the most accurate method to measure elastic modulus of the coating material in this study. However, it could only capable of measuring elastic modulus in transversal direction. Numerical simulation via object orient finite element (OOF) analysis could take to the account pores and splat boundaries, which resulted in a good estimation of the mechanical properties of the coating. OOF results were the closest to the

one obtained from resonance frequency analysis (RFA). According to OOF simulation, the mechanical properties of the coating is lower in longitudinal direction because of the presence of more splat boundaries parallel to coating deposition direction. Estimation of elastic modulus using nanoindentation resulted in highest values that attributed to inability of the technique in including splat boundaries and porosity in the calculation. On the other hand, analytical techniques by using Marshal or Hashin-Hasselman models were resulted in a very low values for elastic modulus. It could be associated with dependency of those methods on hardness values or porosity volume which limited the validity of the models in this special case.

3.8. Acknowledgments

This study was supported by Department of Transportation (DOT) and Pipeline and Hazardous Materials Safety Administration (PHMSA). The authors would also like to acknowledge the help of NDSU Electron Microscopy Center.

CHAPTER 4. THE EFFECTS OF MICROSTRUCTURAL FEATURES ON THE MECHANICAL PROPERTIES OF THE COLD SPRAYED AL-25ZN[2]

4.1. Abstract

In this study, an aluminum matrix composite was fabricated via cold spray deposition technique. Al-25Zn is a good candidate to be applied on the surface of metallic components for corrosion protection. The mechanical stability and performance of such a coating is an important factor during its service life. This study investigates the mechanical behavior of cold sprayed Al-25Zn through experimental, analytical, and numerical simulations. The mechanical properties of coating materials are highly influenced by their microstructural characteristics and therefore, samples were subjected to microstructural characterization using Scanning Electron Microscopy (SEM) and Energy-Dispersive X-ray Spectroscopy (EDS). The hardness of the coating sample was measured using a variety of microhardness tests and were converted to elastic modulus using available analytical models. Experimental tests such as Resonance Frequency Analysis (RFA) and Nanoindentation were conducted to obtain more realistic results for mechanical properties. SEM micrographs were also used for image-based Finite Element Analysis (FEA). Finally, experimental results were compared to the ones obtained from analytical analysis and numerical simulations. Based on the results obtained in this study, it was concluded that the cold sprayed MMCs exhibit an isotropic behavior in the transversal and longitudinal direction. The comparison of the results obtained from the wide range of characterization methods in this study enables researchers in this

[2] The material in this chapter is co-authored by Amir Darabi and Dr. Fardad Azarmi. Amir Darabi wrote this chapter in consultation with Dr. Fardad Azarmi. This chapter is submitted for publication.

field to select the optimum tool and the most accurate method for evaluation of mechanical properties of thermal spraying deposited coating structures.

4.2. Introduction

Metal matrix composites have found a valuable position as crucial components for the industrial products in the past decades. MMCs are known because of their high specific elastic modulus and light weight. The automotive industry, sporting goods, and aircraft manufacturers are widely utilizing MMCs in their products. Of the most used MMCs, particulate–reinforced aluminum matrix is extensively used due to its high specific strength [29, 31, 46-49]. On the other hand, aluminum and zinc alloys are known for their great anti-corrosion properties that makes them the optimum material used for protection of pipelines and steel structures using a method which is known by the industry as "*Metallization*". Zinc-based aluminum alloys have been commercially used for their anti-corrosion properties [21, 50, 51], while aluminum-based alloys have shown good corrosion resistance as well [52]. Among aluminum-based zinc alloys up to 50 vol. % of zinc content, mixtures of aluminum with 20-30 weight percentage of zinc have shown a relatively good mechanical strength [53]. To this end, Al-25 Zn was selected as coating composition in this study.

The common industrial technique for deposition of Al-Zn coating is wire arc spraying. This deposition technique uses wires of Al and Zn or their alloys for development of protective coatings. It is a simple and economically suitable deposition method among different thermal spraying techniques. Furthermore, since it involves melting and solidification of metal, the process is always associated with in-flight oxidation, the formation of unwanted phases, and thickness limitation due to thermal stress build up in the coating during the deposition process. The alternative could be a

spraying method such as *Cold Spraying* which is operational at a lower temperature and does not result in melting and re-solidification of metal [54].

Cold spray technique has been extensively used in recent decades to produce high-quality coatings [55]. While other thermal spraying techniques involve melting and solidification that limits production of thick coatings due to the residual stresses buildup during deposition process, cold spraying is capable of depositing very thick coating layers because it sprays in a solid state [56]. In this process, powders are preheated at temperature ranges below their melting temperature to eliminate humidity and moisture. Then, heated powders are accelerated towards the substrate at very high speeds (300 to 1200 m/s). Powders impact and flatten on the surface of the substrate (target) and the deposited coating layers at high speed. Since the deposition is mainly dependent on the deformation of solid particles, cold spray technique is applicable for ductile materials only. High ductility of aluminum and zinc powders makes them ideal materials to be deposited using cold spray technique.

Cold sprayed coatings are highly reliant on their microstructure since various undesirable features may form during the supersonic spraying of solid particles on the substrate surfaces. Specifically, the existence and distribution of voids, pores, and splat boundaries could significantly influence the quality of the coatings and may alter their physical and mechanical properties. Consequently, understanding the influence of the microstructure on the mechanical properties of cold sprayed MMCs is only achievable through comprehensive characterization of the microstructural features and how they change the mechanical behavior of the composite.

Porosity is one of the most important features that can significantly alter the behavior of the materials and, as a result, should be taken into account while investigating the mechanical properties. Some studies considered only the volume fraction of voids and pores in the

microstructure to predict the mechanical behavior of the composites [57, 58]. This assumption would be insufficient since the location and distribution of these undesirable regions will affect the properties of the composite materials. Some studies offered a more accurate finite element analysis which is dependent on the actual microstructural images from MMCs [59, 60]. Bashirzadeh et al. [29] investigated the relationship between microstructure and mechanical properties of Al-Cu MMCs developed by cold spray technology. However, no numerical simulation can claim an accurate estimation of mechanical properties with respect to the microstructure of the coatings yet [43]. Few published papers have investigated the mechanical properties of Al-Zn alloys or composites [61-63]. It is obvious that a more detailed investigation will contribute to a better understanding of the relationship between microstructural characteristics and properties of cold sprayed MMCs.

This study aims to investigate the mechanical properties such as hardness and elastic modulus of aluminum-based MMCs reinforced with 25 vol. % of zinc deposited by the cold spray deposition technique, in order to address the mechanical behavior of aluminum-zinc metal matrix composites with respect to microstructural features that form during the fabrication process. In this study, numerous techniques, including experimental, analytical, and numerical, were utilized to find the elastic modulus and hardness of the Al-25Zn MMC. The comparison of these results will help to achieve a deeper understanding of the relationship of microstructural formation and mechanical properties of aluminum-based MMC coatings. The obtained results can be used by researchers and industry to be compared to the ones deposited by wire arc spraying or Al-Zn MMCs produced by traditional methods such as casting or powder metallurgy.

4.3. Experimental Procedure

Different mechanical experiments along with analytical and numerical simulations were conducted to measure and validate the mechanical properties of the Al-25Zn MMC. Because of the anisotropic and heterogeneous nature of cold sprayed coatings, it is important to measure properties in both transversal and longitudinal directions. Analytical models were employed to find the Elastic Modulus of the coating using hardness values derived from mechanical experiments. Both Knoop and Vickers hardness tests were conducted for more accurate results. Finally, an image-based finite element model was employed to estimate elastic modulus of the coating using real micrographs taken from coating microstructure. Resonance frequency analysis was applied on free-standing coatings to validate the results obtained from analytical methods, numerical simulations, and mechanical testing.

4.3.1. Materials and Sample Preparation

Aluminum and zinc particles were deposited on the aluminum substrate using cold spraying technique. In this technique, small solid particles of coating materials are accelerated to high velocities (300 to 1200 m/s) towards the substrate without melting, developing a coating on the substrate by an impaction process [8].

Table 4-1. Chemical composition of powders used for cold spray deposition of the coating.

Powder	**Chemical Composition (%)**	**Particle Size**
Aluminum	Al (>99.7), Si (<0.15), Fe (<0.2), Cu (<0.02), Mn (<0.02)	~ 45 (μm)
Zinc	Zn (>99.5), Pb (<0.0018), Fe (<0.0005), Cd (<0.0002)	~ 45 (μm)

As shown in Figure 4-1, the layer-by-layer deposition of semi-molten powders form the coating, although unwanted phases are created during this process.

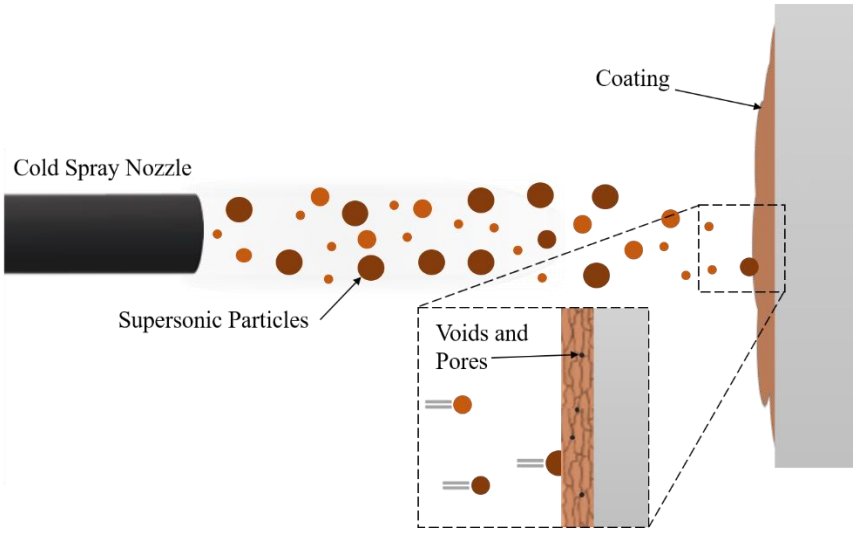

Figure 4-1. Schematic of the cold spraying deposition process.

A PCS1000 Cold Spray equipment (Plasma Giken, Japan) was used to deposit a coating containing commercially available aluminum and zinc powders (Table 4-1) in a ratio of 75 vol. % and 25 vol. %, respectively. The coating was deposited on an aluminum substrate with a size of 40 × 40 × 13 mm, and the thickness of the coating was 1 mm. Table 4-2 shows the operational spraying parameters during the deposition process.

Table 4-2. Parameters of the cold spray deposition process.

Process Parameters	**Value**
Temperature (°C)	400
Pressure (MPa)	3
Powder feeder rate (rpm)	1.8
Processing gas	N2

4.3.2. Microstructural Characterization

Cold spray deposited coatings exhibit a heterogeneous microstructure and it is essential to distinguish different phases and recognize chemical components of the coating by precise microstructural examination. Scanning Electron Microscopy (SEM) was used to have a better perception of the distribution of different phases, as well as the location and percentage of porosities and voids in the coating microstructure. The lower the percentage of voids, the higher

the quality of the coating. The coating was cross-sectioned and mounted in epoxy, then ground and polished prior to the SEM. A JEOL JSM-6490LV SEM (JEOL USA, Peabody MA, USA) was used to perform SEM at a voltage of 15 keV, while a nano-trace Energy-Dispersive X-ray Spectroscopy (EDS) detector was used for elemental analysis on the microstructure; the EDS experiment was performed 9 times at random locations in the coating microstructure. Image analysis was performed on the SEM images in order to obtain the porosity of the deposited coating. Seven different micrographs were studied by iSolution DT software (iMTechnology Co.) according to ASTM E1245 and E562 [31, 32].

4.3.3. Mechanical Testing

4.3.3.1. Knoop indentation

Since its indenter covers a relatively larger area compared to the other indentation tests, the Knoop technique is a favorite method to measure the hardness of coating structures in transversal and longitudinal directions. The wide indentations of the elongated diamond indenter would cover different microstructural features such as splats, pores, voids, and splat boundaries. Therefore, more accurate information regarding the hardness of coating materials can be obtained using this microhardness test. In this study, Knoop indentation was conducted using a Clark CM-800 AT tester under an applied load of 1 kgf for a dwell time of 15 sec. Indentation test was repeated nine times on random regions of the coating microstructure in both transversal and longitudinal directions. The Knoop indentation tests were performed with respect to ASTM E92-17 and the hardness values were calculated using the following equation:

$$HK = \frac{F}{Ap} = \frac{F}{{d_K}^2 \times c_P}, \tag{4-1}$$

where HK is Knoop hardness, F is the applied force in kgf, d_K is the length of the long diagonal, and c_P is the indenter constant, relating the projected area to the square of the long diagonal. Using the ASTM suggested value of 0.07028 for c_P, the equation will be as below:

$$HK = 14.229 \times \frac{F}{{d_K}^2} \tag{4-2}$$

Elastic modulus can be calculated from the measured hardness values obtained from Knoop indentation test using an analytical model developed by Conway [64].

$$\frac{b'}{b} = 1 - 2\left[\left(1-\nu^2\right)\tan\left(\gamma\right)\right]\left(\frac{HK}{E}\right), \tag{4-3}$$

where b and b' are half of the short diagonal of the indenter and indent, respectively, ν is the Poisson ratio of the coating, γ is half of the angle of Knoop indenter, E is the elastic modulus and HK is the Knoop hardness value measured from the test. γ is the average half-angle of a Knoop indenter, assumed to be equal to 75°. It is important to know that Prior to Conway, Marshall et al. [36] has proposed a less complicated equation including parameters such as a and a' that are half of the long diagonal of the indenter and the indent, respectively, and a constant α_1. a' and b' are reported after elastic recovery.

$$E = \frac{\alpha_1 HK}{\frac{b}{a} - \frac{b'}{a'}} \tag{4-4}$$

Leigh et al. [65] indicated that Conway equation is derived from theoretical calculations and showed a large deviation from data points in high values of hardness, while Marshall model could be considered as an empirical approach if α_1 is adjusted to the known data points. The value of constant α_1 was assumed 0.34 as suggested by Meredith et al. [37].

As mentioned in standards, the edge angle of the major Knoop diagonal is 172.5°. As for the minor diagonal, this angle is 130°. Therefore, the ratio of $\frac{b}{a}$ was calculated as:

$$\frac{b}{a} = \frac{\tan\left(\frac{172.5^o}{2}\right)}{\tan\left(\frac{130^o}{2}\right)} = \frac{1}{7.1144} \tag{4-5}$$

4.3.3.2. Vickers Indentation

A Vickers indentation test was conducted on the coating samples to validate the results obtained from the Knoop indentation test. The Vickers hardness test was performed on coating samples by replacing the Knoop indenter with a Vickers indenter on the same Clark Microhardness tester CM-800 AT. A load of 1 kgf with was applied during the Vickers test for 15 sec on the samples. Fifteen Vickers indentations were applied on the cross-section of each coating sample with respect to the ASTM E92-17 standard. 1 kgf was enough to make sure a large area is affected by indentation, which includes voids and splat boundaries.

4.3.3.3. Nanoindentation

Nanoindentation tests are capable of examining mechanical properties from a series of nanoindentations made on the surface of the samples. In this study, a Tribo-Indenter 900 from Hysteron Incorporation was used in quasi-static mode to make indentations in both transversal and longitudinal directions in order to measure the nanohardness on different regions on the cross-section of the coating. To obtain accurate results, thirty indentations were made throughout the sample in each direction. Nanoindentation results can be converted to a specific elastic constant known as reduced elastic modulus. The Eq. (3-6) can be used to calculated elastic modulus from the reduced modulus according to the suggested model by Dejun et al [41].

$$E = \frac{1-\nu^2}{\frac{1}{E_r} - \frac{1-\nu_i^2}{E_i}} \tag{4-6}$$

where E and ν are the elastic modulus and Poisson ratio of the coating, E_i and ν_i are the elastic modulus and Poisson ratio of the diamond indenter, respectively, and E_r is the measured reduced modulus by the Tribo-indenter machine. The elastic constants of the diamond indenter are suggested as $E_i = 1141$ GPa and $\nu_i = 0.07$.

4.3.3.4. Resonance Frequency Analysis

Resonance frequency, also known as *Impulse Excitation*, was conducted on the free-standing Al-Zn MMC coating samples to validate mechanical properties obtained from previous experiments in this study. Important properties such as elastic modulus, shear modulus, and the Poisson ratio of the deposited coating samples can be measured using this technique. Cold sprayed Al-Zn coating was removed from the substrate to form a free-standing sample and cut to the 40 mm × 5 mm × 1.5 mm size. Free-standing coating samples were slightly ground and polished prior to the resonance frequency test to eliminate surface roughness on the surface of the samples to obtain more accurate results. Resonance frequency analysis was conducted according to ASTM E1876-99. This test was performed by a resonance frequency analyzer from IMCE, Belgium. The resonance frequency analyzer performs a non-destructive test in which a hammer continuously taps one side of the specimen, while a microphone detects the induced vibration signals from the other side of the sample. Subsequently, Resonance Frequency Data Analyzer (RFDA) collects the data and converts them to mechanical properties. The average of five repetitions of the test determined the mechanical properties.

4.4. Results

4.4.1. Microstructural Characterization

The microstructural characteristics and properties of the cold sprayed composite coating depends on the chemical composition, purity, and size distribution of the feedstock powders used for the deposition process. The nominal composition and particle geometry have been reported by powder manufacturer as shown in Table 4-2. Fig 2 (a) and (b) (Plasma Giken Co.) shows SEM micrographs of the feedstock powders of aluminum and zinc, respectively. These images were prepared by Plasma Giken Co., LTD. Both powders show relatively high purity with similar size distribution. It can be clearly seen in Figure 4-2 that the aluminum powder is round while zinc exhibit an irregular morphology. Since cold spraying deposition involves high-speed impact and deformation of the particles on the substrate, it is expected that round shape particles could produce a coating with a higher degree of order and better arrangement of the deposited layers [66]. Microstructural observation of the coating microstructure will better reveal the effect of irregularity in Zn particles on the uniformity of the cold sprayed Al-Zn coating.

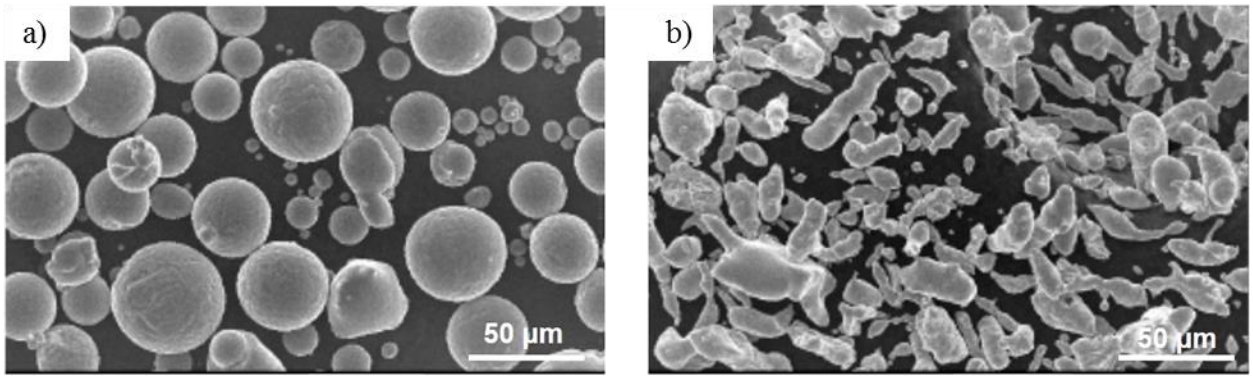

Figure 4-2. SEM micrographs showing the morphology of feedstock powders (a) Aluminum and, (b) Zinc.

SEM images taken from the cross-section of the Al-25Zn coating presented three different contrasts; dark, gray, and light as shown in Figure 4-3. The composition of different contrasts in

the coatings was identified by EDS experiment. Small dark regions represent voids and porosity while dark and light gray regions are Al and Zn, respectively. The average compositions resulted in 99.96±0.02% percent Al in grey regions and 99.41±0.31% percent Zn in light regions. These results are in good agreement with the nominal composition provided by powder manufacturer as listed in Table 4-1. As expected, two different powders used as feedstock were not mixed into one phase and could be recognized as individual phases in the coating microstructure. The light regions that belong to Zn powder were surrounded by dominant grey region representing Al as major phase (matrix). It was speculated that Zn particles were shattered into small particles during impact on the surface. However, image analysis on coating microstructure has shown that the average size of the Zn particles in coating microstructure were in the range of 50 µm. It is close to the nominal size of the Zn feedstock particles as reported by powder manufacturer. The observation of the light regions within the coating microstructure showed that zinc powders kept their original irregular morphology with minimum deformation which could be attributed to the fact that instead of impact on hard surface of the substrate they have landed on sprayed and deformed Al particles with softer surface, resulting in less deformation of the Zn particles.

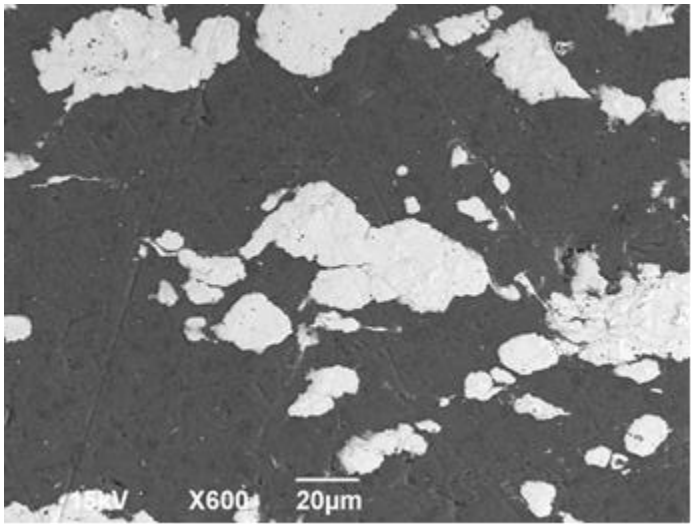

Figure 4-3. SEM micrograph of cold spray deposited Al-25Zn composite.

Porosity measurement using image analysis on several SEM micrographs of cold spraying fabricated coating indicated the existence of 1.26 ± 0.18% porosity and voids in the coating microstructure. The capability of cold spraying in the production of metal matrix composites with a very low amount of porosity has also been previously reported for both low and high pressure modes [29, 67]. This could be attributed to the elimination of voids and porosity formation during melting and solidification process which is a big source of porosity formation in most of the thermal spraying techniques. In addition, EDS measurements determined the existence of 25.28±1.64% of zinc in the coating microstructure, showing a good agreement with the nominal composition of Al-25Zn.

4.4.2. Knoop Indentation

SEM micrograph shown in Figure 4-4 illustrates a Knoop indent on the cross-section of the coating. The average hardness value for the cold sprayed Al-25Zn coating based on nine indentations was 57.94±1.73 HK and 59.50±1.68 HK in transversal and longitudinal directions, respectively.

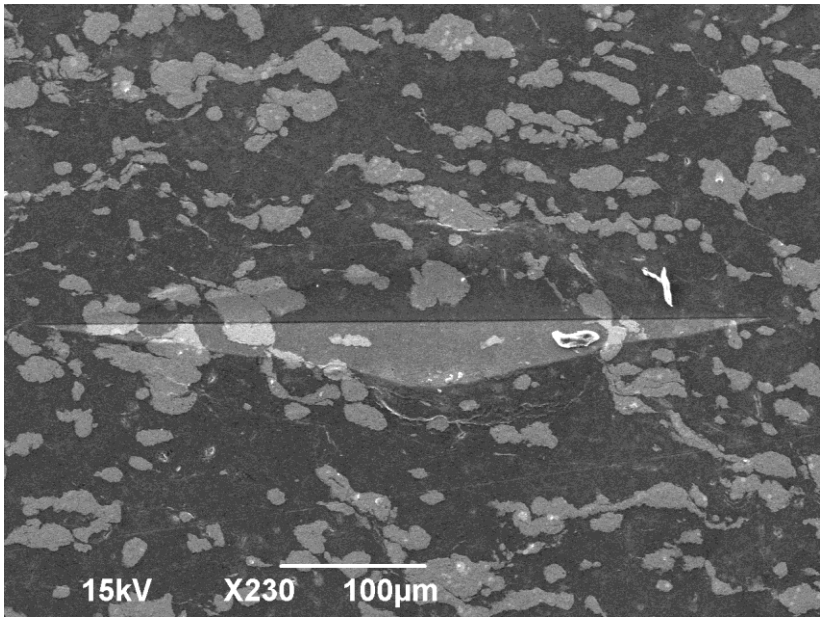

Figure 4-4. Knoop indentation on the cross section of cold sprayed Al-25Zn coating.

Marshall's equation (Eq. 3-4) could convert the hardness value to elastic modulus. The calculated modulus of elasticity was 33.70±3.51 GPa in transversal and 41.51±6.75 GPa in longitudinal directions. The high value of standard deviation in longitudinal direction corresponds to scattering hardness values. It is also attributed to the high sensitivity of the Marshall equation to the diagonal width of the indentation which is measured in microns. Figure 4-5 shows the measured hardness values and their corresponding elastic modulus.

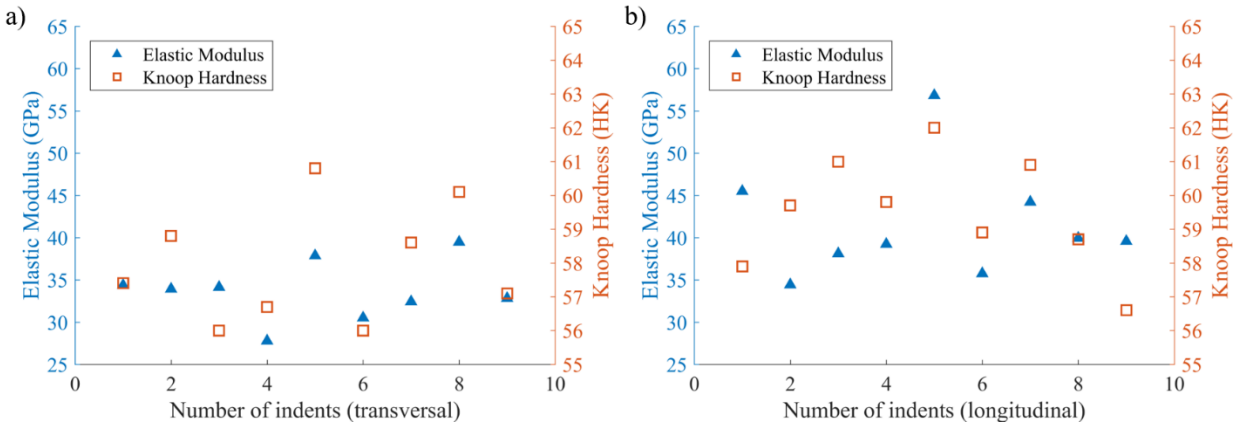

Figure 4-5. Knoop hardness and elastic modulus measurements in (a) transversal, (b) longitudinal directions.

4.4.3. Vickers Indentation

Vickers microhardness test was conducted to validate the obtained results from Knoop indentation on Al-Zn coating samples. The measured hardness value was 54.42±2.43 HV. Due to the diamond shape of Vickers indenter, there is no need to perform it in different (longitudinal or transverse) directions. Savaşkan *et al.* [53] obtained a microhardness of around 110 HV for Al-25Zn alloy. Comparing the results of the microhardness measurements with the literature, it is noticeable that the hardness value of the deposited coating is lower than the Al-25Zn sample produced by mold casting process. This could be due to the microstructural features such as porosities that are formed more frequently during the deposition of the coating. However, the results are in an acceptable range for thermal spray coatings considering the composition of the cold sprayed coating [68].

4.4.4. Nanoindentation

A total of 60 indents in longitudinal and transversal directions were made by the Berkovich indenter on the coating cross section during the nanoindentation experiment. The large number of indentations is to guarantee that the hardness of entire microstructure including all phases, interfaces, and voids is measured and the nanoscale indenter covers a large distance within the microstructure. Three loading stages were used during nanoindentation experiment. In the first five seconds, the load was increased from 0 to 1000 μN and then, it was kept constant for a dwell time of five seconds. Finally, the load was gradually removed and decreased to zero in five seconds. Hardness values can be directly obtained from the nanoindentation equipment. However, during nanoindentation test, both indenter and sample experience deformation which needed to be taken to the account. According to the hardness results and deformation in sample and indenter, the machine calculates a mechanical constant known as reduced modulus, which is a combination

of elastic deformation in the indenter and the coating sample [40]. In this study, the obtained reduced modulus was converted to the elastic modulus as explained in 4.3.3.3.

The measured values of hardness were 1.04±0.17 GPa and 0.92±0.37 GPa in transversal and longitudinal directions, respectively. The calculated elastic modulus using Eq. (3-6) were 71.42±5.00 GPa and 69.28± 11.96 GPa in transversal and longitudinal directions, respectively. Fig. 6 shows the load-displacement curves obtained from the nanoindentation test in both transversal and longitudinal directions. As it is clear from this graph, the coating experiences less displacement in the transversal direction and this can be translated to the higher strength and elastic modulus.

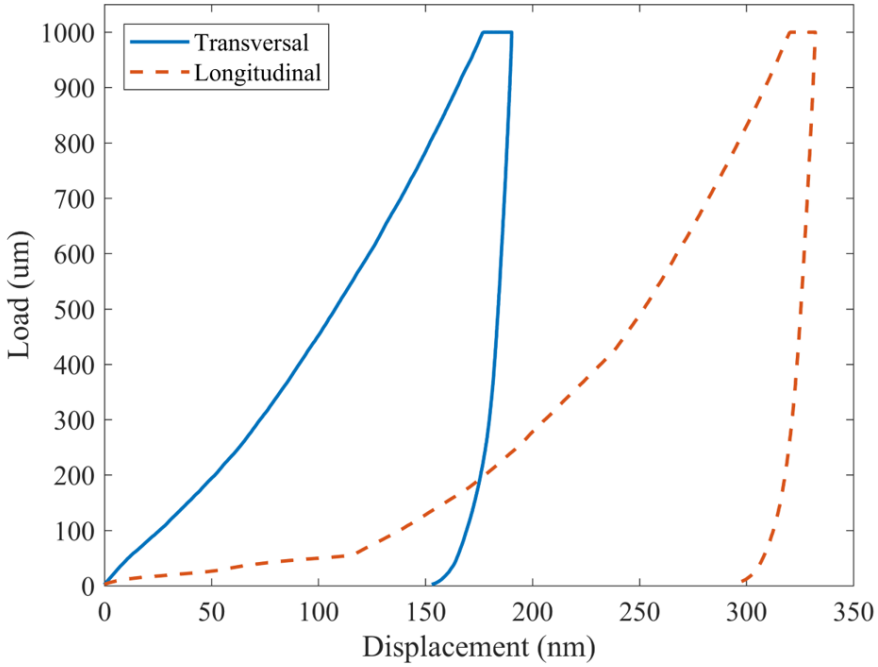

Figure 4-6. Load-Displacement curves of the transversal and longitudinal nanoindentations.

4.4.5. Resonance Frequency Analysis

Resonance frequency test was performed 5 times on a free-standing Al-25 Zn coating sample to measure the mechanical properties of the coating in the transverse direction. The

measured elastic modulus and Poisson ratio were 35.63±0.01 GPa, and 0.231. Resonance frequency has the most accurate results and could be used as a reference for comparing with other results and measurements.

4.5. Numerical Simulation

Various *Finite Element Analysis (FEA)* packages are commercially available to examine the mechanical properties of homogenous materials independent of their microstructural characteristics [69]. On the other hand, the mechanical behavior of inhomogeneous materials is mostly dependent on their microstructural features. Cold spray deposited Al-Zn coating is a great example of inhomogeneous materials with anisotropic properties. Object-Oriented Finite (OOF) element, developed by US National Institute Standards and Technology (NIST), offers an image-based FEA simulation that utilizes actual microstructural images for numerical simulation. Therefore, high-quality micrographs are used for a comprehensive evaluation of mechanical properties by taking to the account microstructural features such as pores, voids, and interface of different regions through numerical simulations.

In this study, high-resolution SEM images, taken from random locations of the coating cross-section at the same magnification, were subjected to object-oriented finite element analysis. Figure 4-8 (a) exhibits an SEM micrograph selected for finite element analysis in this study. Each image consists of thousands of pixels that were divided into different groups based on their contrast. Black pixels were assigned to the voids and pores, dark gray represents the aluminum matrix, and light gray belongs to the zinc. This classification is performed according to the results obtained from EDS experiment and image analysis. Several assumptions for threshold values of each contrast was made to distinguish porosity pixels from those corresponding to the matrix material. Figure 4-7 shows the area fraction of black pixels to the total number of pixels and their

comparison with respect to the measured porosity of the coating obtained by image analysis. In this figure, threshold 1 had the best agreement with the porosity level resulted from image analysis performed on the samples.

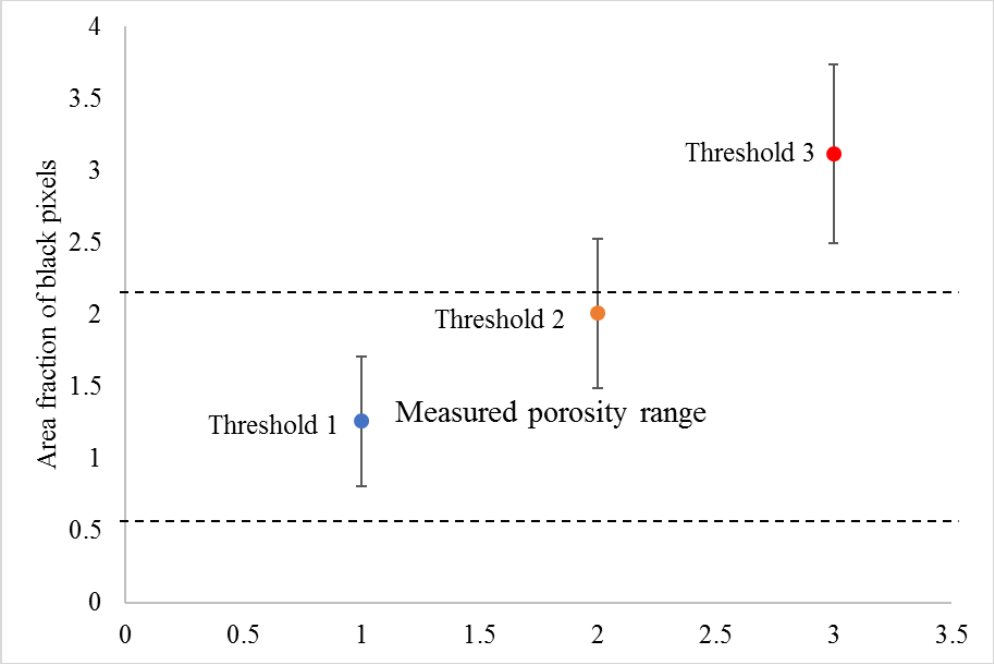

Figure 4-7. Comparison of three contrast thresholds with respect to the coating porosity.

Each group of pixels was assigned properties such as elastic modulus and Poisson ratio based on the material they are representing. The assigned properties to each pixel group are listed in Table 4-3. A very small value was assigned to the elastic modulus of the group representing pores and voids, since a value of zero is not accepted by the software. In addition to mechanical properties, certain contrasts were assigned to each group to better distinguish the different regions in the microstructure. The processed image created from SEM micrograph is shown in Figure 4-8 (b).

Table 4-3. Mechanical properties assigned to each contrast and pixel group.

Group	Assigned Material	Elastic Modulus (GPa)	Poisson Ratio
Dark Gray	Aluminum	70	0.34
Light Gray	Zinc	100	0.25
Black	Pores and Voids	E-9	0.3

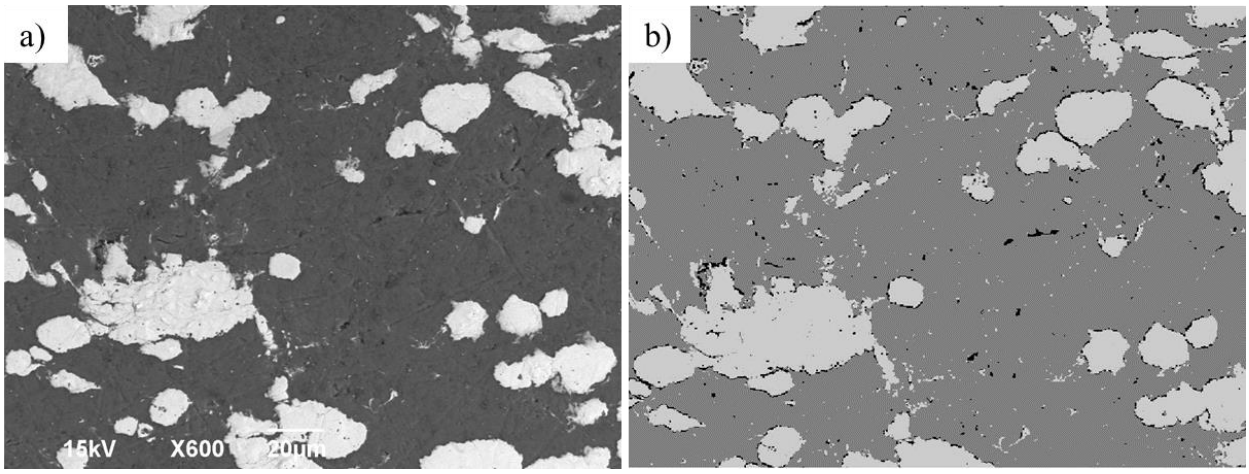

Figure 4-8. (a) An example of SEM micrographs used for object-oriented FEA study, (b) processed image according to the assigned properties to each contrast.

In the next step, a skeleton of triangular elements is built upon the micrograph which is shown in Figure 4-9 (a). A skeleton is a structure of elements and the final mesh is generated based on the skeleton created in this stage. There are certain tools available in the software to modify and improve the quality of the skeleton. These modifications are necessary to increase the homogeneity of elements by dividing them into multiple smaller elements. Each iteration of modification increases the number of elements, resulting in higher accuracy and consequently, an increase in simulation time. In this process, modifications were performed in two steps; first, the elements that contained pixels from multiple groups were cut to smaller ones through refining, and in the second step, all edges of individual elements were aligned with the interfacial boundaries between different pixel groups by application of annealing process. Figure 4-9 shows the step by step development and modification of a skeleton on the micrograph of the cold sprayed sample. The refined and annealed images (skeleton) are shown in Figure 4-9 (b and c). To better show the

changes applied to elements and their geometry, a selected part of the skeleton marked in Figure 4-9 (c) has been shown in higher magnification in Figure 4-9 (d). The modification resulted in an increase in the homogeneity of elements to 98.2%. The higher the homogeneity of the pixels, the better the accuracy of the FEA solution.

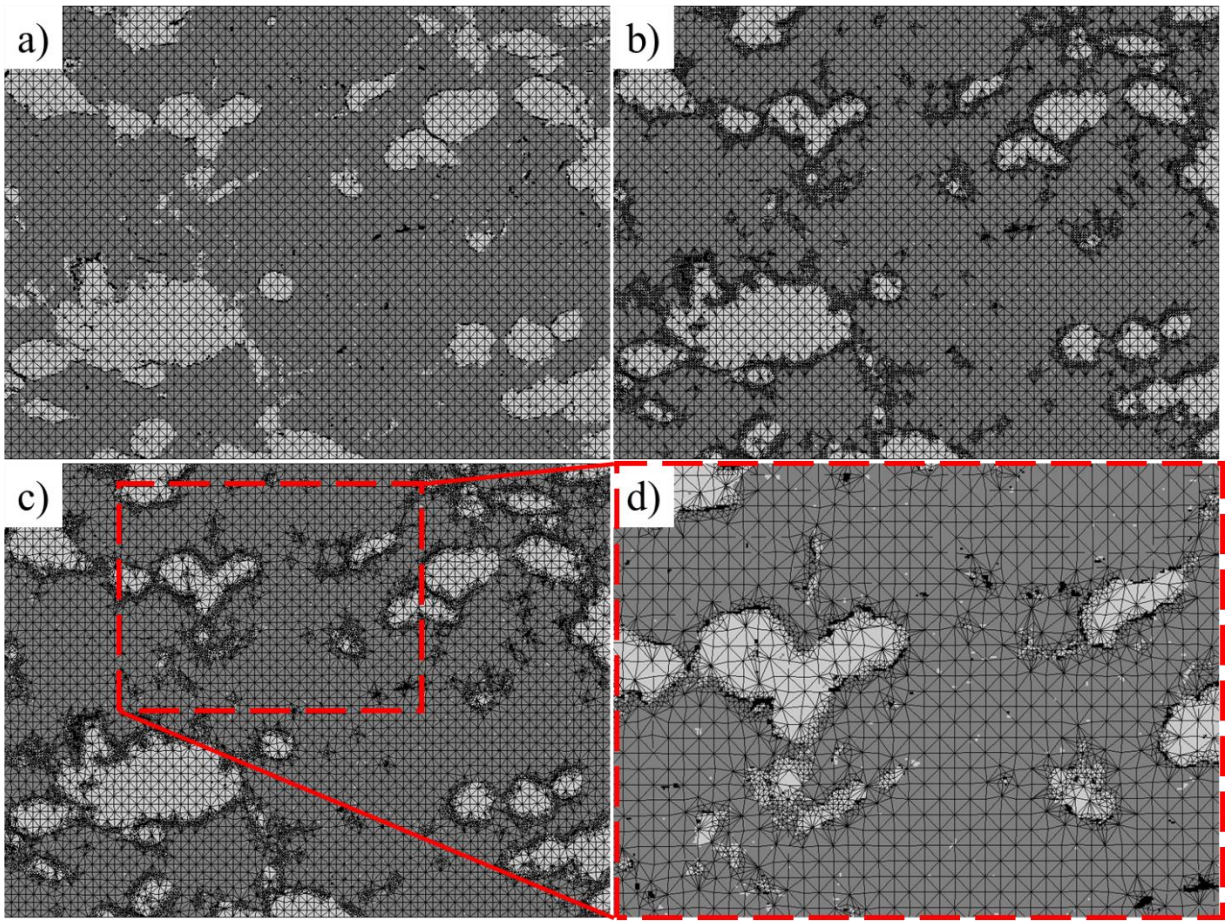

Figure 4-9. Modifications on the skeleton built on the micrograph. a) Skeleton built on n_x=90 and n_y=60 elements b) refined skeleton c) annealed skeleton and d) a higher magnification view of selected section as marked in (c).

Then, a mesh system was generated on the skeleton and boundary conditions were applied to the discretized elemental system. In this study, top and bottom boundaries were assumed to be free, the left boundary was fixed, and a small displacement was applied on the right boundary to ensure no plastic deformation occurs. Finally, by solving a *Force Balance* problem on the mesh,

OOF reported the average values of stress and strain over the entire mesh. Inserting stress and strain values in the x-direction (transversal) into the constitutive relation of a plane stress condition and biaxial stresses (Eq. 3-7 [44]) will yield the value of elastic modulus. Poisson ratio is calculated using the rule of mixture.

$$E = \frac{\sigma_{xx}(1-\nu)}{\varepsilon_{xx}} \tag{4-7}$$

This simulation is performed on three micrographs taken randomly from different regions of the coating cross-section microstructure to increase the accuracy of this image-based FEA study. The estimated elastic modulus of the coating sample was calculated as 57.75±0.51 GPa and 57.76±0.71 GPa in transversal and longitudinal directions, respectively. Figure 4-10 shows the stress distribution obtained by OOF.

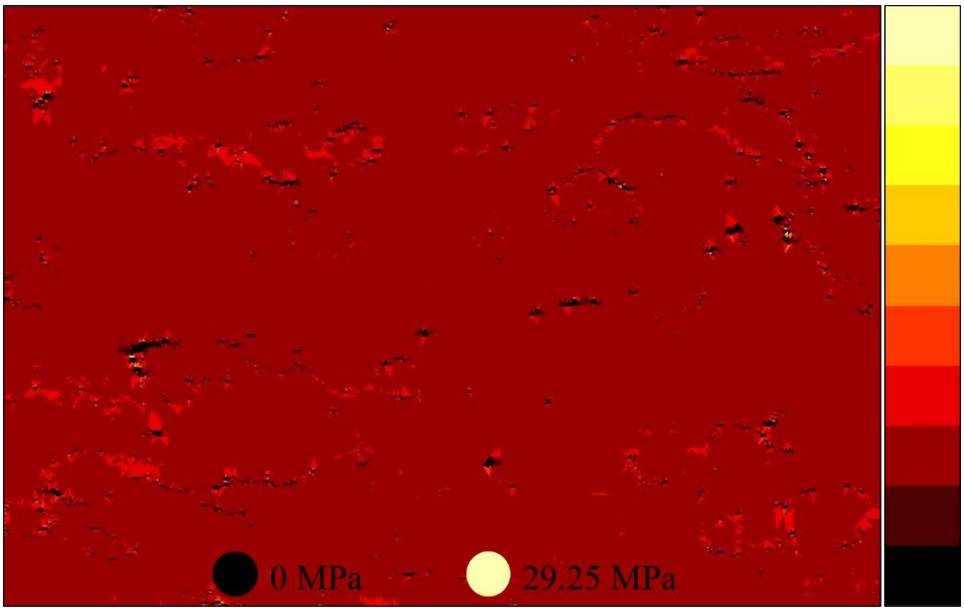

Figure 4-10. Stress distribution map for Al-25Zn coating micrograph as analyzed by OOF.

4.6. Analytical Analysis

Typically, the properties of coatings deposited by thermal spray technology are mostly dependent on their microstructure since they have a certain amount porosity and unwanted phases compared to fully dense materials. As a result, coatings exhibit a very different mechanical behavior than conventionally processed materials with a homogenous structure. There are plenty of analytical methods that relate the mechanical properties to the microstructure of a material. Hashin and Shtrikman [70] developed a model for two-phased particle-reinforced MMCs which measures the elastic modulus of the composite by knowing the values of bulk and shear moduli of both particle and matrix.

$$K^H = K_P + \frac{\nu_M}{\frac{1}{K_M - K_P} + \frac{3\nu_P}{3K_P + 4G_P}} \tag{4-8}$$

$$K^L = K_M + \frac{\nu_P}{\frac{1}{K_P - K_M} + \frac{3\nu_M}{3K_M + 4G_M}} \tag{4-9}$$

$$G^H = G_P + \frac{\nu_M}{\frac{1}{G_M - G_P} + \frac{6\nu_P\left(K_P + 2G_P\right)}{5G_P\left(3K_P + 4G_P\right)}} \tag{4-10}$$

$$G^L = G_M + \frac{\nu_P}{\frac{1}{G_P - G_M} + \frac{6\nu_M\left(K_M + 2G_M\right)}{5G_M\left(3K_M + 4G_M\right)}} \tag{4-11}$$

where ν is the volume fraction, K is bulk modulus, and G is shear modulus. Subscripts M and P refer to matrix and particle, respectively, while superscripts H and L show the higher and lower bound estimates. Calculation of these values using the bulk modulus, shear modulus, and Poisson ratio of aluminum (matrix) and zinc (particle) showed that higher and lower bound estimates are

very close. Therefore, an average value was used to calculate the elastic modulus of the composite, E_C:

$$E_c = \frac{9K}{1+\frac{3K}{G}}, \tag{4-12}$$

which yields 76.39 GPa for Al-25Zn fully dense composite without porosity. This model cannot be reliable since thermal spray coatings always exhibit a porous microstructure and, therefore, dissimilar mechanical behavior. A model was proposed by Hashin-Hasselman [45] that measures the elastic modulus of a porous material using the following equation:

$$E = E_0\left[1+\frac{Ap}{1-(A+1)\,p}\right], \tag{4-13}$$

where E_0 is the elastic modulus of the bulk material, A is a constant equal to -33.4, and p is the porosity. The rule of mixture is employed to calculate E_0 of Al-25Zn.

$$\log E_0 = \nu_{Al}\log E_{Al} + \nu_{Zn}\log E_{Zn} \tag{4-14}$$

Using Hashin-Hasselman model, an elastic modulus of 53.66 GPa is obtained.

4.7. Discussion

Table 4-4 lists the results obtained from experimental, analytical, and numerical simulation used in this study to determine the elastic modulus of cold sprayed Al-25Zn MMC.

Table 4-4. Elastic modulus of Cold Sprayed Al-25Zn measured with various methods.

Method	$\boldsymbol{E_T}$ Transversal (GPa)	$\boldsymbol{E_L}$ Longitudinal (GPa)
Resonance frequency analysis	35.63±0.01	-
Nanoindentation	71.42±5.00	69.28±11.28
Marshall's equation	33.70±3.51	41.51±6.75
Hashin-Shtrikman model	76.39	-
Hashin-Hasselman model	53.66	-
OOF	57.75±0.51	57.76±0.71

The elastic modulus obtained from resonance frequency analysis is the most accurate result among the various methods that were conducted in this study. Due to the anisotropic nature of the coating materials, it has been tried to perform tests and analysis to measure the elasticity in both transversal and longitudinal directions. However, resonance frequency analysis is only capable of such a measurement in the transverse direction. The unidirectional measurement of elastic modulus also applies to analytical methods such as Hashin-Hesselman and Hashin-Shtrikman. On the hand, nanoindentation, Marshall from Knoop indentation, and numerical simulation by OOF could measure the elasticity in both directions.

It is noticeable that the elastic modulus obtained from Marshall's equation is in very good agreement with those obtained from resonance frequency analysis. The model proposed by Marshall uses the hardness values obtained from the Knoop hardness test and since its indenter can cover most of the existing features within the coating microstructure, a detail overall estimation of elastic modulus is expected from application of this model. Nanoindentation has reported significantly higher values for elastic modulus compared to the other experimental measurements. This could be due to the fact that the nano-scale measurement in this test. The results may be derived from indentations landing on individual phases without taking to the account interfacial properties between different regions of the microstructure.

In the next step, available analytical models proposed for composites and coating materials were employed to estimate mechanical properties of the cold sprayed Al-25Zn. An Analytical model such as Hashin-Shtrikman idealized the coating microstructure by neglecting the presence of pores and voids and resulted in an overestimation of the elastic modulus. On the other hand, the model developed by Hashin-Hasselman included the volume of the voids and porosity and provided a better estimation of elastic modulus compared to the one obtained from Hashin-

Shtrikman. Furthermore, Hashin-Hasselman still lacks to include the distribution, geometry, and aspect ratio of the porosity in the model which can be the reason for its deviation from the accurate results.

Object oriented finite element analysis predicted elastic modulus in a similar range as estimated by Hashin-Hasselman model. However, it is approximately, 60% higher than the more accurate values obtained from resonance frequency and Marshall's equation. This could be attributed to the fact that the image-based scheme was unable to collect all microstructural features that could influence mechanical properties due to the quality of pictures and the contrasts. Another reason could be the inability of the program to properly define interfacial regions and discretized elements between the aluminum matrix and zins particles. In addition, prediction of a 3-dimensional material property such as elastic modulus from information collected from a 2D image cannot provide the highest accuracy.

Altogether, due to the isotropic nature of this OOF simulation, and since cold sprayed Al-25Zn coating contained low porosity, the measured elastic moduli for both longitudinal and transversal directions were almost equal. The important factors that could influence the estimated values of elastic modulus at different directions are the existence of higher splat boundaries in longitudinal directions and different aspect ratio of the particles. No visible splat boundaries were observed in the micrographs and zinc particles kept the semi-circular geometry within the microstructure. These two factors contributed to the similar elastic modulus calculated in both directions in this study.

4.8. Conclusion

This study tries to evaluate the mechanical properties of Al-25Zn composite material deposited via cold spraying technique. A combination of experimental study, numerical

simulation, and analytical methods were used to address the mechanical strength of the coating material. This study pays special attention to the influence of microstructural characteristics on the mechanical behavior of the samples. Resonance frequency analysis provided the most accurate results for mechanical properties. A semi experimental-analytical method developed by Marshall which uses hardness values of the material obtained from Knoop indentation in an analytical model also provided accurate results in this study. However, the nanoindentation experimental study could not precisely measure the elastic modulus of the coating material. This was attributed to the small size of the Berkovich indenter used in this experiment. The indenter was not capable of capturing information from interfacial regions between the matrix and particulate reinforcement phases. Among the analytical models utilized in this study, the one which ignored microstructural features such as voids and porosity could not predict mechanical properties accurately while the one considering those features in their calculations provided more realistic results. Finally, object-oriented finite element analysis estimated approximately %60 higher elastic modulus for Al-25Zn coating. It is due to limitations of this technique in capturing all microstructural features such as splat boundaries and cracks in the coating microstructure. In general, the estimation of mechanical behavior of coating structures is a challenging task and results obtained from this study could help to select more appropriate methods for evaluation of their mechanical properties and performance.

4.9. Acknowledgements

This study was funded by Department of Transportation (DOT) and Pipeline and Hazardous Materials Safety Administration (PHMSA). The authors would also like to acknowledge the help of NDSU Electron Microscopy Center.

CHAPTER 5. COMPARISON OF THE COATINGS

Previous chapters thoroughly investigated the mechanical properties and the microstructural features of aluminum-zinc coatings deposited by two different thermal spray techniques; wire arc spraying and cold spraying. As it was mentioned previously in the "general Introduction" section, this study tries to investigate possibilities of replacing wire arc sprayed Zn-15Al coating with the cold spray deposited Al-25 Zn coating. To this end, in this chapter, these two coatings will be compared in three different categories. First, important microstructural characteristics which may define coating thermo-mechanical properties are compared between the two coatings. Second, the mechanical properties such as hardness and elastic modulus of the both coatings are investigated. Finally, the coatings are subjected to a corrosion test to determine their durability and resistance in corrosive environments.

5.1. Microstructural Comparison

Figure 5-1 (a & b) show an SEM micrograph from the cross section of wire arc spray Zn-15Al and cold spray deposited Al-25Zn, respectively. It is noticeable that the porosity level is much less in the coating deposited by cold spray technique. Using available image analysis tools, the porosity of the wire arc deposited Zn-15Al coating is $7.35 \pm 0.93\%$, while this amount is equal to $1.38 \pm 0.75\%$ for the cold sprayed Al-25Zn. This significant difference between the amounts of the porosities have made major impact on the coating properties deposited by wire arc spraying method. The influence of porosity level on mechanical properties of both coatings will be discussed in section 5.2. SEM images of the wire arc sprayed coating (Figure 5-1 a) show that the porosities are mostly oriented in the transversal direction along the splat boundaries, significantly affecting the elastic modulus in the longitudinal direction.

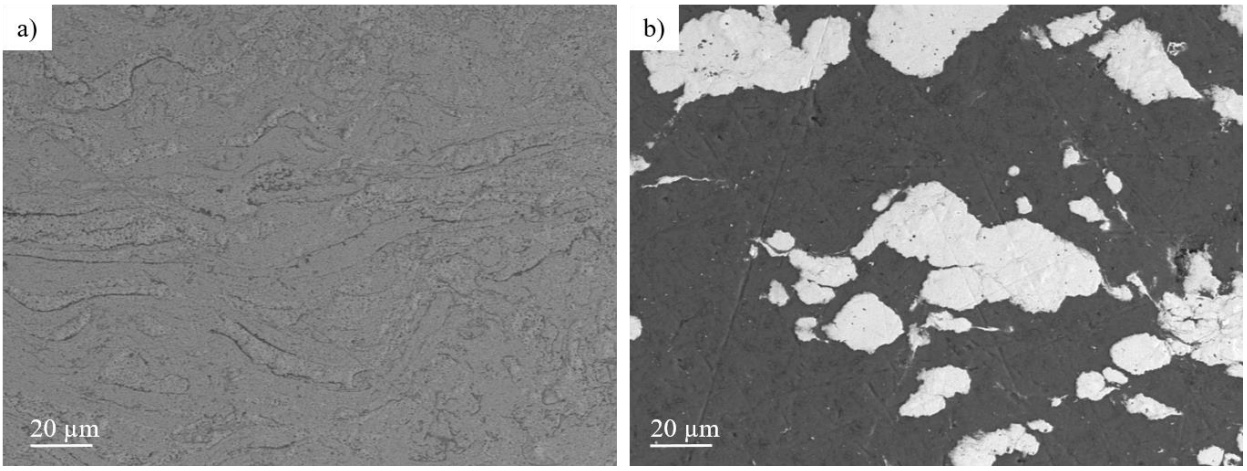

Figure 5-1. SEM micrographs of a) wire arc sprayed Zn-15Al and b) cold sprayed Al-25Zn.

The high porosity in the microstructure of the wire arc deposits has led to the formation of large and irregularly-shaped voids, as shown in Figure 5-2 (a). The presence of voids causes stress concentrations that may finally lead to the failure of the coating. On the other hand, the microstructure of the cold sprayed coating contains much less voids, and the existing voids have smaller size and a more rounded profile compared to those from the wire arc deposited coating. As a result, there are more stress concentration points in the microstructure of the wire arc deposited coating, which cause major influences on its mechanical behavior.

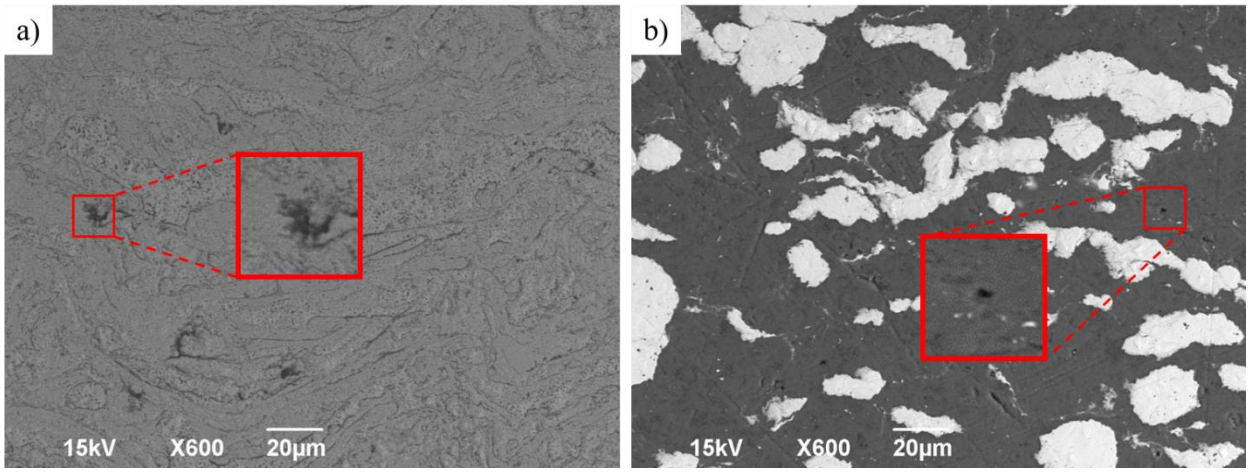

Figure 5-2. Void shape and size in the microstructure of a) wire arc deposited and b) cold sprayed coatings.

Several SEM micrographs were taken from the interfacial boundary regions between the both coating samples and the substrates to investigate the coating's adhesion to the substrate. Figure 5-3 (a-d) show micrographs from the cross section of the coating and substrate interface for both type of coating samples. A noticeable difference can be detected between the two coating samples in terms of interfacial adhesion. It is predictable that wire arc deposited sample shows weaker adhesion to the substrate (Figure 5-3 a) due to the formation of large porosities and voids which were formed during the impact of the first layer splats to the substrate surface. Several factors such as large thermal gradients between substrate and coating or splashing of molten particles during impact could result in formation of those voids in the interfacial regions of the wire arc sprayed coating as shown with higher magnification in (Figure 5-3 a and c). On the other hand, the bonding mechanism of the cold spray deposition is dependent on the high velocity impact of the solid particles with the surface of the substrate. The deformation caused by the impact lead to the build-up of the coating layers without provoking any thermal stresses, which minimizes the formation of voids and pores (Figure 5-3 b and d). As a result, a uniform interfacial region with minimum visible voids resulted from utilizing the cold spray method, which may result in stronger interfacial adhesion between coating and substrate.

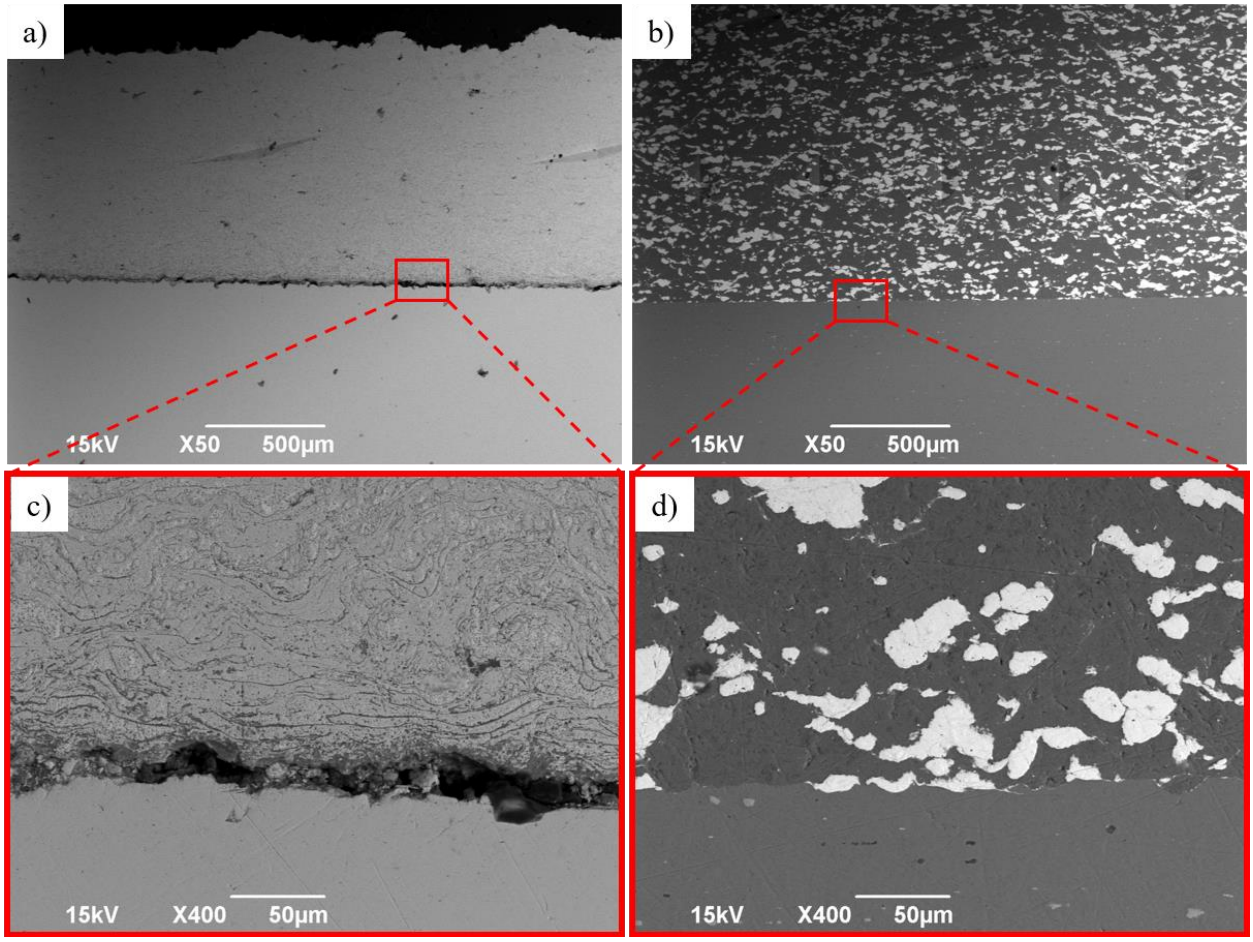

Figure 5-3. SEM micrographs of the interfacial boundary between the coating and the substrate. a & c) wire arc sprayed Zn-15Al and b & d) cold sprayed Al-25Zn deposits.

5.2. Mechanical Comparison

Chapters two and three have deeply discussed the mechanical properties of the wire arc sprayed Zn-15Al and cold sprayed Al-25Zn, respectively. The hardness and elastic modulus of the coating samples were measured using experimental methods such as Knoop and Vickers microhardness techniques, nanoindentation test, and resonance frequency analysis. The hardness and elastic modulus obtained from these mechanical experiments will be further evaluated and compared to better understand the capability of each technique to produce coatings with superior mechanical properties, resulting in longer service life and durability.

5.2.1. Hardness

Table 5-1 lists the results obtained for the microhardness measurements on both coating samples using Knoop and Vickers indentation tests as mentioned in previous chapters. Both hardness tests indicated higher hardness for the cold sprayed coating. For more accurate comparison and better understanding of each coating, it is important to consider the hardness of aluminum and zinc, and also their alloys. There are many sources available in the literature that report the hardness of aluminum-zinc alloys. The reported values are ranging from 14 HV (commercially pure aluminum) to 150 HV (Zn-4Al alloy 2, pressure die casting) [42]. Hardness is very dependent on the fabrication process of the materials. The measured Vickers hardness values lie in the range reported by various sources. But the trend of the HV hardness values shows that higher amount of zinc, usually increases the material hardness, given the same manufacturing process.

The higher hardness of the cold sprayed coating, with lower percentage of zinc, indicates that the cold spraying could deposit coatings with higher quality (lower porosity level) that result in higher hardness values compared to the one produced by wire arc spraying.

Table 5-1. Mechanical properties of the coating samples obtained by microhardness indentation.

Mechanical Property	**Zn-15Al Wire Arc Deposit**	**Al-25Zn Cold Spray Deposit**
Knoop Transversal	46.83 ± 1.94	57.94 ± 1.73
Knoop Longitudinal	44.83 ± 0.97	59.50 ± 1.68
Vickers	45.29 ± 1.70	54.42 ± 2.43

5.2.2. Elastic Modulus

SEM observations indicated that the microstructure of the coating samples contain a certain amount of porosity that differ based on the deposition method. The presence of porosity influences the mechanical properties of the coatings, and the elastic modulus of the wire arc sprayed coating was significantly affected by the pores and voids that formed during deposition. Since zinc has a

higher elastic modulus compared to aluminum [71], the wire arc deposited coating with higher amount of zinc in the its matrix (85%) is expected to show higher elastic modulus compared to the cold sprayed coating with less amount of zinc (25%). However, as shown by the numerical simulations, coatings from both techniques have almost the same elastic modulus in transversal direction, while in longitudinal direction the elastic modulus is even higher for the cold sprayed coating. As discussed in the previous section, the porosities in the microstructure of the wire arc sprayed sample were mostly oriented in the transversal direction. Therefore, the elastic modulus of the coating was significantly lower than expected in the longitudinal direction.

The Resonance Frequency Analysis (RFA) and nanoindentation are two mechanical experiments that could directly measure the elastic modulus of the coating samples in this study. Overall, RFA has measured higher elastic modulus for the wire arc sprayed coating sample in the transversal direction. The measured elastic moduli were 51.27 GPa for the Zn-15Al wire arc sprayed coating, and 51.27 GPa for the Al-25Zn cold sprayed coating sample. This method has the highest accuracy between the mechanical experiments performed in this study, but the limitation of this method is the inability to measure the elastic modulus of the coating in the longitudinal direction.

Nanoindentation experiment has reported values that have overestimated the elastic modulus of the coating samples. This overestimation may be due to the fact that each indent covers a nano-scale area and is only made on a specific region on the microstructure (such as a zinc or aluminum particle, or voids and splat boundaries). As a result, the obtained hardness values from nanoindentation experiment may not be a good representation of the overall mechanical properties of thermal sprayed coatings with inhomogeneous structure containing features such as porosity, voids, and splat boundaries at micron scale.

The elastic modulus of the coating samples resulted from nanoindentation test as previously mentioned in chapter two and chapter three are listed in Table 5-2 The elastic modulus of zinc and aluminum are reported by the literature are approximately 100 GPa and 70 GPa, respectively. Since the wire arc sprayed coating sample include almost three times more zinc compared to the cold sprayed one, it was expected to obtain higher elastic modulus for Zn-15Al coating deposited by wire arc spraying method. However, the effect of the splat boundaries is noticeable in the results of elastic modulus measurements in the longitudinal direction, as it is around 20% lower than the elastic modulus in the transversal direction. As for the cold sprayed sample, the measured values for elastic modulus are very close. Therefore, it can be concluded that the cold sprayed coating exhibits an isotropic behavior, which has also been confirmed by numerical simulation on the cold sprayed sample. This isotropic behavior can be resulted from the rounded shape of zinc powders in the aluminum matrix of the cold sprayed sample, along with very low amount of porosity that is distributed over the microstructure with no specific orientation (compared to the wire arc deposited coating sample).

Table 5-2. Elastic modulus measured by nanoindentation for both coating samples.

Coating Type	E_T **Transversal (GPa)**	E_L **Longitudinal (GPa)**
Zn-15Al Wire Arc Deposit	87.58 ± 13.07	71.07 ± 16.41
Al-25Zn Cold Spray Deposit	71.42 ± 5.00	69.28 ± 11.28

5.3. Corrosion Comparison

Both coating samples were subjected to an electrochemical test with a setup shown in Figure 5-4 to determine the corrosion performance of the wire arc deposited and cold sprayed AL-Zn coatings. The PVC pipes were adhered to the coating using Loctite epoxy and these pipes were filled with 3.5wt% NaCl solution as electrolyte for electrochemical corrosion test. To prevent any leakage during the test, samples were cured for 24 hours in room temperature to obtain the

maximum bounding strength of adhesive. Then, a conductive wire was attached to the bottom of the sample to provide electrical connection between the testing instruments.

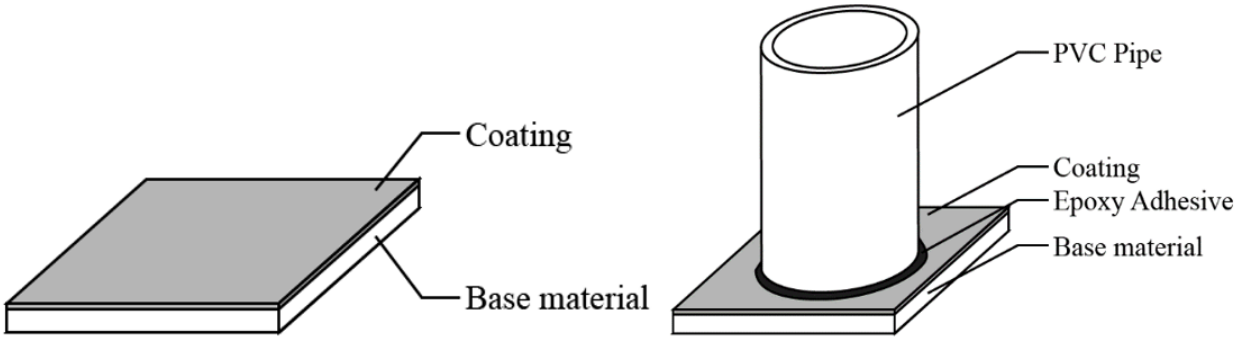

Figure 5-4. The corrosion test setup on the coating samples.

Accelerated electrochemical corrosion test was carried out with a Gamry Reference 600 Ptentiostat/Galvanostat/ZRA instrument. Working electrode was first connected to a generic electric wire, and the wire was attached to the bottom side of sample for better connectivity (due to thickness of the samples, clips of working electrode cannot be applied to samples directly). Platinum was used as inert metal, and AgCl with KCl solution were used in reference bar which was calibrated before the test. The overal schematic of the experiment is shown in Figure -5-5.

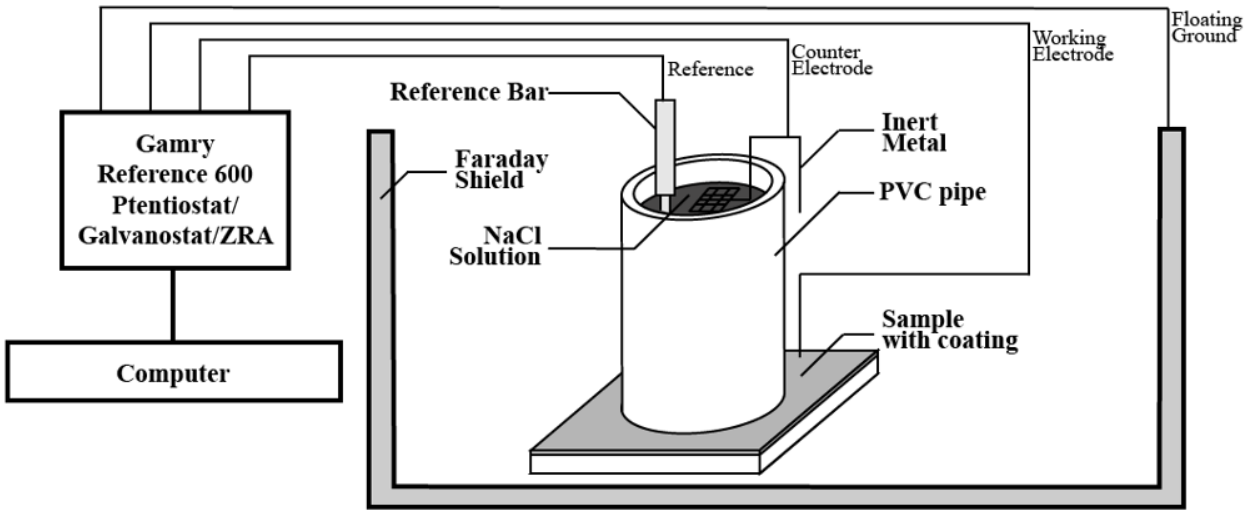

Figure -5-5. Schematic of the electrochemical experiment on coating samples.

The Tafel test results for the cold sprayed Al-25Zn coating sample are shown in Figure 5-6 (a). The lowest point of the curve indicated that anodic reaction and cathodic reaction reach an equilibrium. The corresponding potential at that lowest point was open circuit potential or corrosion potential. Tafel fit was conducted on the linear part of both cathodic and anodic range. Thus, two straight lines representing cathodic and anodic current should be carried out. The corresponding current to the intersection of these two straight lines is corrosion current. The slope of anodic range (called Tafel parameter A), together with corrosion potential and corrosion current, serve as three major indicators for corrosion resistance in Tafel test. The resultant corrosion current and corrosion voltage were 7.1 μA and 1.2 V, respectively. Same experiment was conducted on the substrate of the coating samples as well as the wire arc deposited Zn-15Al coating. Figure 5-6 (b) illustrates Tafel curve of wire arc deposited Zn-15 Al coating. The measured corrosion current was in the range of 700 nA, while the corrosion voltage was equal to 1.22V.

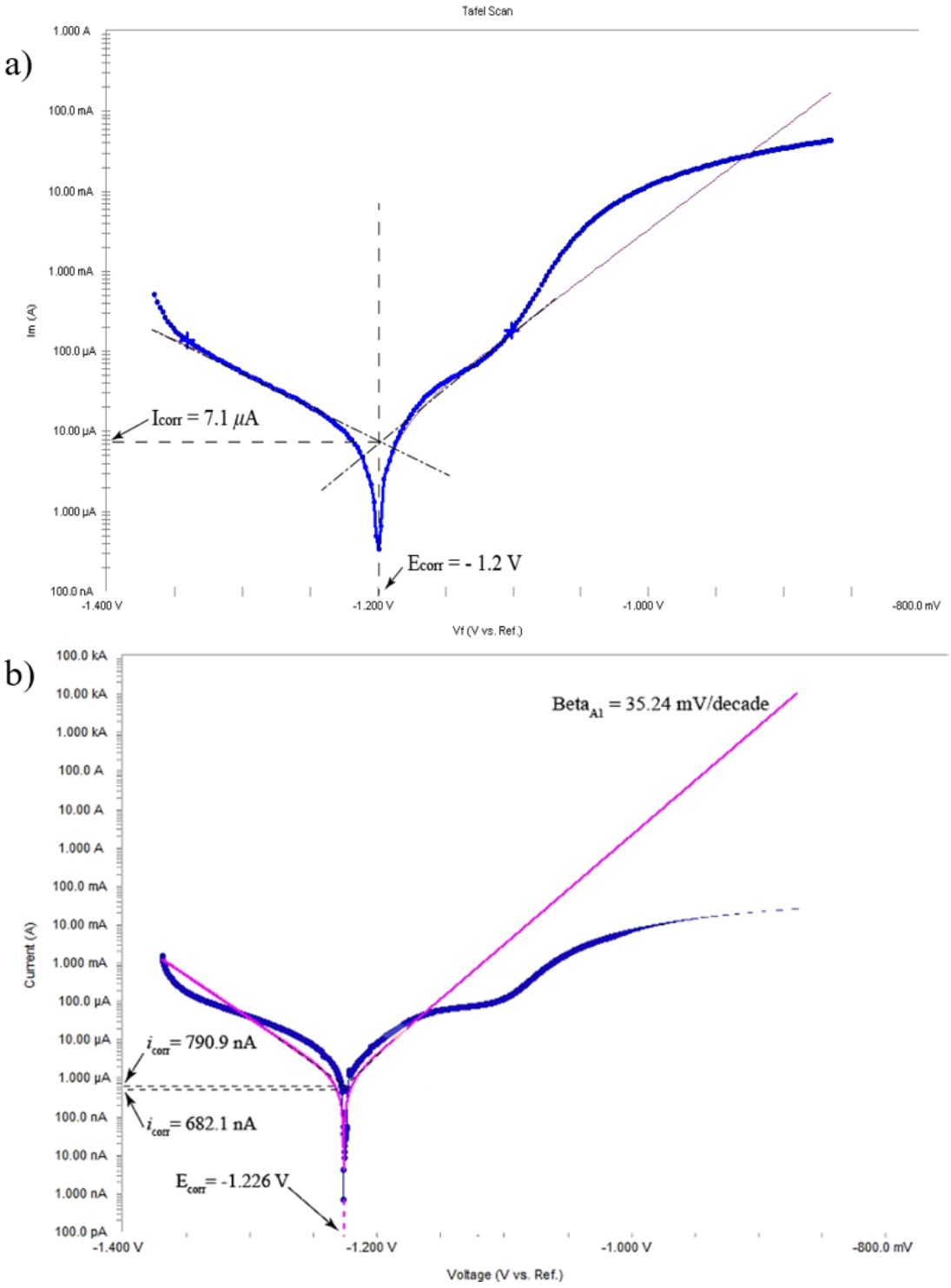

Figure 5-6. Tafel curve of a) the cold sprayed Al-25Zn coating and b) the wire arc sprayed coating.

Table 5-3 lists the corrosion parameters and the corrosion rate of the substrate, cold sprayed Al-25Zn, and wire arc deposited Zn-15Al. Both thermal spray coating samples have improved the corrosion resistance of the base material over three times. However, wire arc sprayed Zn-15Al has shown the lowest corrosion rate of 0.11 mill/year, which is up to ten times better than the substrate. A corrosion rate of 0.11 mpy is well below the concerned range of corrosion.

Table 5-3. Corrosion performance comparison between the substrate and the deposited thermal spray coatings.

Material	Corrosion Potential, Ecorr (mv)	Corrosion Current Density, icorr ($\mu A/cm^2$)	Corrosion Rate (mill/year)
Substrate	-1062	638.3	1.82
Wire Arc deposited Zn-15Al	-1173	0.736	0.11
Cold sprayed Al-25Zn	-1200	7.1	0.595

The results of corrosion experiment indicated that both coatings are capable of providing protection for the substrate against corrosion. Zinc and aluminum are of the most common materials for corrosion protection because of their low electronegativity. Additional amount of zinc in the wire arc sprayed coating sample resulted in better corrosion resistance, although the cold sprayed sample had better quality in terms of mechanical properties and microstructural features.

CHAPTER 6. GENERAL CONCLUSION AND FUTURE RECOMMENDATIONS

This chapter aims to briefly conclude the subjects of previous chapters and address the future steps that can be taken into account to further continue this study.

6.1. General Conclusion

The main goal of this study was to investigate the possibility of finding an alternative coating system (materials and technology) to the currently used metallization technique which is commonly used for applying coating against corrosion in pipeline industry. Zinc based coating s are deposited via wire arc spraying in metallization technology. An alternative coating system by utilizing cold spraying to deposit Aluminum based coatings has been examined in this study. To this end a comprehensive study was performed to measure important microstructural, mechanical, and electrochemical properties of both coatings followed by a complete comparison of these properties. In general, thermal spray coatings have porous and inhomogeneous microstructure that vary depending on the deposition method. There are several techniques of thermal spraying to produce coatings such as plasma spraying, high velocity oxygen fuel (HVOF), wire arc spraying, cold spraying, and flame spraying.

For each type of coating, the mechanical properties such as hardness and elastic modulus were measured using various mechanical experiments. Resonance frequency analysis, nanoindentation, Knoop and Vickers indentation are among the experiments performed in this study. Cold spray coating sample exhibited higher hardness values compared to the wire arc spray deposited coating. During deposition and solidification process of wire arc spraying method, the high temperature of molten particles resulted in development of thermal stresses that may influence the coating build up process. However, wire arc sprayed Zn-15 Al showed a higher elastic modulus since it contained approximately three times more zinc (with higher elastic modulus than

aluminum) in its composition compared to the cold sprayed Al-25 Zn. The lower porosity level of cold sprayed sample reduced the significant effect of Zinc in the calculated elastic moduli between two samples.

Microstructural characterization is an essential investigation in order to identify the effect of inhomogeneous microstructure of thermal spray coatings on their mechanical behavior. Therefore, both coatings were studied by employing scanning electron microscopy (SEM) on the cross section of coating samples. In addition, image analysis determined the porosity level of each coating sample. Microstructural examination indicated that the wire arc deposition method develops coatings with considerable volume of unwanted microstructural features. These features are mostly pores, splat boundaries, and voids. According the microstructural observations, the stronger interfacial adhesion between coating and substrate in cold spray deposited coating is due to existence of very low amount of porosity and void in this region compared to the one produced by wire arc spraying.

Electrochemical testing was conducted on both coating samples to evaluate the corrosion resistance of the coating samples. The results indicated that the coating with higher amount of zinc (Zn-15Al) has superior anti-corrosion properties, although the cold sprayed coating (Al-25Zn) was also capable of reducing the corrosion rate of the substrate material up to three times.

Considering all the aforementioned discussions, it can be concluded that the coatings deposited by cold spraying technique are high-quality dense coatings with good interfacial adhesion to the substrate. The deposition process has a very low impact on the mechanical behavior of the coatings, such as hardness. Furthermore, the porosity is very low compared to other affordable thermal spraying techniques. On the other hand, the material Zn-15Al has proven to be a better aluminum-zinc alloy compared to Al-25Zn, in terms of elastic modulus and corrosion

resistance. Therefore, a Zn-15Al coating deposited by cold spraying technique can be a new approach for metallization of the surface of industrial parts and components, including oil and gas pipelines, considering the fact that the mobile cold spray equipment can produce high-quality deposits of anti-corrosive Zn-15Al material.

6.2. Future Recommendations

There are several aspects that can be taken into account for the next steps of this study. From mechanical aspect, following experiments can help for a more accurate measurement of mechanical properties of the coatings:

1- Three-point and four-point bending tests on the samples to find the fracture toughness of the coating.

2- Tensile test in case of permeability of preparing T-bone test specimens to determine the elastic modulus of in transversal direction.

3- Peel-off test to determine the interfacial adhesion toughness of the coating to the substrate.

Additional investigations can be performed in terms of microstructural characterization. AFM is one of the most capable instruments for microstructural investigations that can be utilized find out surface morphology and intergranular cracking [72-74]. AFM can also be used to map the topography of the coating samples during the electrochemical experiment [75].

Finally, developing of a new coating with the composition of Zn-15Al by via cold spray deposition method is suggested as promising possible alternative to the current metallization technique. The same study can be applied on different types of coatings to validate the results from this study. It is speculated that a cold sprayed Zn-15Al coating exhibits good mechanical properties, as well as good corrosion resistance.

REFERENCES

[1] Davis, S. C., 1999, "Transportation Energy Data Book, Edition 19," Oak Ridge National Lab., TN (US).

[2] Wang, H., Yajima, A., Liang*, R. Y., and Castaneda, H., 2015, "Bayesian modeling of external corrosion in underground pipelines based on the integration of Markov chain Monte Carlo techniques and clustered inspection data," Computer-Aided Civil and Infrastructure Engineering, 30(4), pp. 300-316.

[3] Peabody, A. W., 1967, Control of pipeline corrosion, National Association of corrosion engineers Houston, Texas.

[4] Revie, R. W., 2008, Corrosion and corrosion control: an introduction to corrosion science and engineering, John Wiley & Sons.

[5] Wrobleski, D. A., Benicewicz, B. C., Thompson, K. G., and Bryan, C. J., 1997, "Corrosion resistant coating," Google Patents.

[6] Tanaka, J., Ono, K., Hayashi, S., Ohsasa, K., and Narita, T., 2002, "Effect of Mg and Si on the microstructure and corrosion behavior of Zn–Al hot dip coatings on low carbon steel," ISIJ international, 42(1), pp. 80-85.

[7] Pawlowski, L., 2008, The science and engineering of thermal spray coatings, John Wiley & Sons.

[8] Davis, J. R., 2004, Handbook of thermal spray technology, ASM international.

[9] Heimann, R. B., 2008, Plasma-spray coating: principles and applications, John Wiley & Sons.

[10] Souza, V., and Neville, A., 2005, "Corrosion and synergy in a WCCoCr HVOF thermal spray coating—understanding their role in erosion–corrosion degradation," Wear, 259(1-6), pp. 171-180.

[11] Toriz, F., Thakker, A., and Gupta, S., "Thermal barrier coatings for jet engines," Proc. ASME 1988 International Gas Turbine and Aeroengine Congress and Exposition, American Society of Mechanical Engineers, pp. V005T013A012-V005T013A012.

[12] Fauchais, P. L., Heberlein, J. V., and Boulos, M. I., 2014, "Wire Arc Spraying," Thermal Spray Fundamentals, Springer, pp. 577-629.

[13] Michlik, P., and Berndt, C., 2006, "Image-based extended finite element modeling of thermal barrier coatings," Surface and Coatings Technology, 201(6), pp. 2369-2380.

[14] Nakamura, T., Qian, G., and Berndt, C. C., 2000, "Effects of Pores on Mechanical Properties of Plasma-Sprayed Ceramic Coatings," Journal of the American Ceramic Society, 83(3), pp. 578-584.

[15] Lee, W. Y., Stinton, D. P., Berndt, C. C., Erdogan, F., Lee, Y. D., and Mutasim, Z., 1996, "Concept of functionally graded materials for advanced thermal barrier coating applications," Journal of the American Ceramic Society, 79(12), pp. 3003-3012.

[16] Esfahani, E. A., Salimijazi, H., Golozar, M. A., Mostaghimi, J., and Pershin, L., 2012, "Study of corrosion behavior of arc sprayed aluminum coating on mild steel," Journal of thermal spray technology, 21(6), pp. 1195-1202.

[17] Kuroda, S., Kawakita, J., and Takemoto, M., 2006, "An 18-year exposure test of thermal-sprayed Zn, Al, and Zn-Al coatings in marine environment," Corrosion, 62(7), pp. 635-647.

[18] Szymański, K., Hernas, A., Moskal, G., and Myalska, H., 2015, "Thermally sprayed coatings resistant to erosion and corrosion for power plant boilers-a review," Surface and Coatings Technology, 268, pp. 153-164.

[19] Okyere, M. S., 2019, Corrosion Protection for the Oil and Gas Industry: Pipelines, Subsea Equipment, and Structures, CRC Press.

[20] Gusev, V., Nesterenko, N., Il'ichev, M., Konovalov, P., and Tyuftyaev, A., 2018, "Study of Coating Corrosion Resistance for Shelf Structural Objects and Oil Industry Equipment," Chemical and Petroleum Engineering, 53(11-12), pp. 745-749.

[21] De Rincón, O., Rincón, A., Sánchez, M., Romero, N., Salas, O., Delgado, R., López, B., Uruchurtu, J., Marroco, M., and Panosian, Z., 2009, "Evaluating Zn, Al and Al–Zn coatings on carbon steel in a special atmosphere," Construction and Building Materials, 23(3), pp. 1465-1471.

[22] Gulec, A., Cevher, O., Turk, A., Ustel, F., and Yilmaz, F., 2011, "Accelerated Corrosion Behaviors of Zn, Al and Zn/15Al Coatings on a Steel Surface," Materiali in tehnologije, 45(5), pp. 477-482.

[23] Fayomi, O., and Popoola, M., 2012, "Comparative studies of microstructural, tribological and corrosion properties of plated Zn and Zn-alloy coatings," International Journal of Electrochemical Science, 7, pp. 4860-4870.

[24] Schwingel, D., Taylor, R., Haubold, T., Wigren, J., and Gualco, C., 1998, "Mechanical and thermophysical properties of thick PYSZ thermal barrier coatings: correlation with microstructure and spraying parameters," Surface and Coatings Technology, 108, pp. 99-106.

[25] Kweh, S., Khor, K., and Cheang, P., 2000, "Plasma-sprayed hydroxyapatite (HA) coatings with flame-spheroidized feedstock: microstructure and mechanical properties," Biomaterials, 21(12), pp. 1223-1234.

[26] Lima, R., Karthikeyan, J., Kay, C., Lindemann, J., and Berndt, C., 2002, "Microstructural characteristics of cold-sprayed nanostructured WC–Co coatings," Thin solid films, 416(1-2), pp. 129-135.

[27] Deshpande, S., Kulkarni, A., Sampath, S., and Herman, H., 2004, "Application of image analysis for characterization of porosity in thermal spray coatings and correlation with small angle neutron scattering," Surface and coatings technology, 187(1), pp. 6-16.

[28] Eslaminejad, A., Ramzanpour, M., Hosseini-Farid, M., Ziejewski, M., and Karami, G., 2018, "Cerebrospinal Fluid-Skull Interaction Analysis for A Non-Invasive Intracranial Monitoring Technique." Biomedical Sciences Instrumentation, 57(1), pp. 69-75.

[29] Bashirzadeh, M., Azarmi, F., Leither, C., and Karami, G., 2013, "Investigation on relationship between mechanical properties and microstructural characteristics of metal matrix composites fabricated by cold spraying technique," Applied Surface Science, 275, pp. 208-216.

[30] Wang, Z., Kulkarni, A., Deshpande, S., Nakamura, T., and Herman, H., 2003, "Effects of pores and interfaces on effective properties of plasma sprayed zirconia coatings," Acta Materialia, 51(18), pp. 5319-5334.

[31] Jahani, B., Salimi Jazi, M., Azarmi, F., and Croll, A., 2018, "Effect of volume fraction of reinforcement phase on mechanical behavior of ultra-high-temperature composite consisting of iron matrix and TiB2 particulates," Journal of Composite Materials, 52(5), pp. 609-620.

[32] ASTM E-03, 2003, "Standard Practice for Determining the Inclusion or Second-Phase Constituent Content of Metals by Automatic Image Analysis."

[33] Ang, A. S. M., and Berndt, C. C., 2014, "A review of testing methods for thermal spray coatings," International Materials Reviews, 59(4), pp. 179-223.

[34] Leither, C., Risan, J., Bashirzadeh, M., and Azarmi, F., 2013, "Determination of the elastic modulus of wire arc sprayed alloy 625 using experimental, analytical, and numerical simulations," Surface and Coatings Technology, 235, pp. 611-619.

[35] Meyers, M. A., and Chawla, K. K., "Mechanical behavior of materials, 2009," Google Scholar.

[36] Marshall, D. B., Noma, T., and Evans, A. G., 1982, "A Simple Method for Determining Elastic-Modulus–to-Hardness Ratios using Knoop Indentation Measurements," Journal of the American Ceramic Society, 65(10), pp. c175-c176.

[37] Meredith, N., Sherriff, M., Setchell, D., and Swanson, S., 1996, "Measurement of the microhardness and Young's modulus of human enamel and dentine using an indentation technique," Archives of Oral Biology, 41(6), pp. 539-545.

[38] Zhang, Y., Yang, L., Zeng, X., Zheng, B., and Song, Z., 2013, "The mechanism of anneal-hardening phenomenon in extruded Zn–Al alloys," Materials & Design, 50, pp. 223-229.

[39] Chicot, D., Ageorges, H., Voda, M., Louis, G., Dhia, M. B., Palacio, C., and Kossman, S., 2015, "Hardness of thermal sprayed coatings: Relevance of the scale of measurement," Surface and Coatings Technology, 268, pp. 173-179.

[40] Shuman, D. J., Costa, A. L., and Andrade, M. S., 2007, "Calculating the elastic modulus from nanoindentation and microindentation reload curves," Materials characterization, 58(4), pp. 380-389.

[41] Dejun, M., Wo, O. C., Liu, J., and Jiawen, H., 2004, "Determination of Young's modulus by nanoindentation," Science in China Series E: Technological Sciences, 47(4), pp. 398-408.

[42] 2018, "CES Edupack 2018," Granta Design.

[43] Azarmi, F., Coyle, T., and Mostaghimi, J., 2009, "Young's modulus measurement and study of the relationship between mechanical properties and microstructure of air plasma sprayed alloy 625," Surface and Coatings Technology, 203(8), pp. 1045-1054.

[44] Hsueh, C. H., Haynes, J. A., Lance, M. J., Becher, P. F., Ferber, M. K., Fuller, E. R., Langer, S. A., Carter, W. C., and Cannon, W. R., 1999, "Effects of interface roughness on residual stresses in thermal barrier coatings," Journal of the American Ceramic Society, 82(4), pp. 1073-1075.

[45] Hashin, Z., 1962, "The elastic moduli of heterogeneous materials," Journal of Applied Mechanics, 29(1), pp. 143-150.

[46] Siriyala, R., Alluru, G. K., Penmetsa, R. M. R., and Duraiselvam, M., 2012, "Application of grey-taguchi method for optimization of dry sliding wear properties of aluminum MMCs," Frontiers of Mechanical Engineering, 7(3), pp. 279-287.

[47] Rajesh, S., Krishna, A. G., Raju, P. R. M., and Duraiselvam, M., 2014, "Statistical analysis of dry sliding wear behavior of graphite reinforced aluminum MMCs," Procedia materials science, 6, pp. 1110-1120.

[48] Songmene, V., and Balazinski, M., 1999, "Machinability of graphitic metal matrix composites as a function of reinforcing particles," CIRP Annals-Manufacturing Technology, 48(1), pp. 77-80.

[49] Bobić, B., Mitrović, S., Babić, M., and Bobić, I., 2010, "Corrosion of metal-matrix composites with aluminium alloy substrate," Tribology in industry, 32(1), pp. 3-11.

[50] Shaw, B. A., and Moran, P. J., 1985, "Characterization of the corrosion behavior of zinc-aluminum thermal spray coatings."

[51] McCune, R. C., Ricketts, M. S., Gao, G., Neiser, R. A., Puskar, J., and Roemer, T. J., 2003, "Selective galvanizing using kinetic spraying," No. 0148-7191, SAE Technical Paper.

[52] Davis, J. R., 1999, Corrosion of aluminum and aluminum alloys, Asm International.

[53] Savaşkan, T., Bican, O., and Alemdağ, Y., 2009, "Developing aluminium–zinc-based a new alloy for tribological applications," Journal of materials science, 44(8), pp. 1969-1976.

[54] Stoltenhoff, T., Kreye, H., and Richter, H., 2002, "An analysis of the cold spray process and its coatings," Journal of Thermal Spray Technology, 11(4), pp. 542-550.

[55] Moridi, A., Hassani-Gangaraj, S. M., Guagliano, M., and Dao, M., 2014, "Cold spray coating: review of material systems and future perspectives," Surface Engineering, 30(6), pp. 369-395.

[56] Stokes, J., and Looney, L., 2004, "Residual stress in HVOF thermally sprayed thick deposits," Surface and Coatings Technology, 177, pp. 18-23.

[57] Li, C., Ohmori, A., and McPherson, R., 1997, "The relationship between microstructure and Young's modulus of thermally sprayed ceramic coatings," Journal of materials Science, 32(4), pp. 997-1004.

[58] Li, C., He, Y., and Ohmori, A., "Characterization of structure of thermally sprayed coating," Proc. Thermal spray: Meeting the challenges of the 21st Century,(ed) C. Coddet,(pub) ASM International, Materials Park, OH, USA, pp. 717-722.

[59] Chawla, N., Sidhu, R., and Ganesh, V., 2006, "Three-dimensional visualization and microstructure-based modeling of deformation in particle-reinforced composites," Acta Materialia, 54(6), pp. 1541-1548.

[60] Kenesei, P., Borbely, A., and Biermann, H., 2004, "Microstructure based three-dimensional finite element modeling of particulate reinforced metal–matrix composites," Materials Science and Engineering: A, 387, pp. 852-856.

[61] Baris, A., Chinh, N., Valiev, R., and Langdon, T., 2015, "Microstructure decomposition and unique mechanical properties in an ultrafine-grained Al-Zn alloy processed by high-pressure torsion," Kovove Mater, 53(4), pp. 251-258.

[62] Liu, C., Qu, B., Ma, Z., Ma, M., and Liu, R., 2016, "Recrystallization, precipitation, and resultant mechanical properties of rolled Al–Zn alloy after aging," Materials Science and Engineering: A, 657, pp. 284-290.

[63] Kanth, U. R., Rao, P. S., and Krishna, M. G., 2018, "Mechanical behaviour of fly ash/SiC particles reinforced Al-Zn alloy-based metal matrix composites fabricated by stir casting method," Journal of Materials Research and Technology.

[64] Conway, J., 1986, "Determination of hardness to elastic modulus ratios using Knoop indentation measurements and a model based on loading and reloading half-cycles," Journal of materials science, 21(7), pp. 2525-2527.

[65] Leigh, S. H., Lin, C. K., and Berndt, C. C., 1997, "Elastic response of thermal spray deposits under indentation tests," Journal of the American Ceramic Society, 80(8), pp. 2093-2099.

[66] Papyrin, A., Kosarev, V., Klinkov, S., Alkhimov, A., and Fomin, V. M., 2006, Cold spray technology, Elsevier.

[67] Azarmi, F., Tangpong, X., and Chandanayaka, T., 2015, "Investigation on mechanical properties of cold sprayed Ni–Ni3Al composites," Surface Engineering, 31(11), pp. 832-839.

[68] Dzhurinskiy, D., Maeva, E., Leshchinsky, E., and Maev, R. G., 2012, "Corrosion protection of light alloys using low pressure cold spray," Journal of thermal spray technology, 21(2), pp. 304-313.

[69] Eslaminejad, A., Hosseini-Farid, M., Ramzanpour, M., Ziejewski, M., and Karami, G., "Determination of Mechanical Properties of Human Skull With Modal Analysis," Proc. ASME 2018 International Mechanical Engineering Congress and Exposition, American Society of Mechanical Engineers, pp. V003T004A097-V003T004A097.

[70] Hashin, Z., and Shtrikman, S., 1963, "A variational approach to the theory of the elastic behaviour of multiphase materials," Journal of the Mechanics and Physics of Solids, 11(2), pp. 127-140.

[71] Callister, W. D., and Rethwisch, D. G., 2007, Materials science and engineering: an introduction, John Wiley & Sons New York.

[72] Li, G.-R., Yang, G.-J., Li, C.-X., and Li, C.-J., 2017, "A comprehensive mechanism for the sintering of plasma-sprayed nanostructured thermal barrier coatings," Ceramics International, 43(13), pp. 9600-9615.

[73] Kim, D.-Y., Joshi, B. N., Lee, J.-G., Lee, J.-H., Lee, J. S., Hwang, Y. K., Chang, J.-S., Al-Deyab, S., Tan, J.-C., and Yoon, S. S., 2016, "Supersonic cold spraying for zeolitic metal–organic framework films," Chemical Engineering Journal, 295, pp. 49-56.

[74] Ji, X., Li, X., Yu, H., Zhang, W., and Dong, H., 2019, "Study on the carbon nanotubes reinforced nanocomposite coatings," Diamond and Related Materials, 91, pp. 247-254.

[75] Perry, J. M., Hodgkiess, T., and Neville, A., 2002, "A comparison of the corrosion behavior of WC-Co-Cr and WC-Co HVOF thermally sprayed coatings by in situ atomic force microscopy (AFM)," Journal of thermal spray technology, 11(4), pp. 536-541.

APPENDIX

In this study, the goal is to find out the mechanical behaviors of the coating under different experimental tests. Both wear and Rockwell hardness tests were carried out and results are discussed in the following paragraphs.

Wear test determines the behavior of the coating in physical contact with other objects which may result in friction and abrasion and material loss over time. Hardness test can show the resistance of the coating to any indentation and deformation. The wear test is performed in the UMT DFH20G Bruker machine, which can apply up to 200 N force. This device can measure Sliding Wear and Friction Behavior between a Static Pin (Area Contact) or Ball (Point Contact) and a Rotating Surface. For this experiment, the indenter applied a load of 10 N, rotating on a circle with a diameter of 2 cm at 265 rpm for 80 min, corresponds to a total distance of 1332 m.

Table A-1. Coefficient of friction resulted from wear test on Zn-15Al wire arc sprayed coating.

Surface of Wear Test	**F_x**	**F_z**	**COF**
Zn-15Al Coating	4.186±1.018	10.18±1.787	0.4121±0.071
Aluminum Substrate	4.87±0.6088	9.966±0.635	0.4883±0.501

The hardness test was carried out using a Rockwell tester at load of 100 kgf and a steel ball with a diameter of 1.588 mm. Rockwell is a fast method, developed for production control and it has a direct readout. Because of the effects of the corrosion and the wear tests on the coating, there are three regions on the sample, outside of the glued region (R1), inside of the glued region (R2), and the worn-out region (R3) caused by the wear test. The hardness test was performed on each region. Figure 5 shows different regions of sample under hardness test.

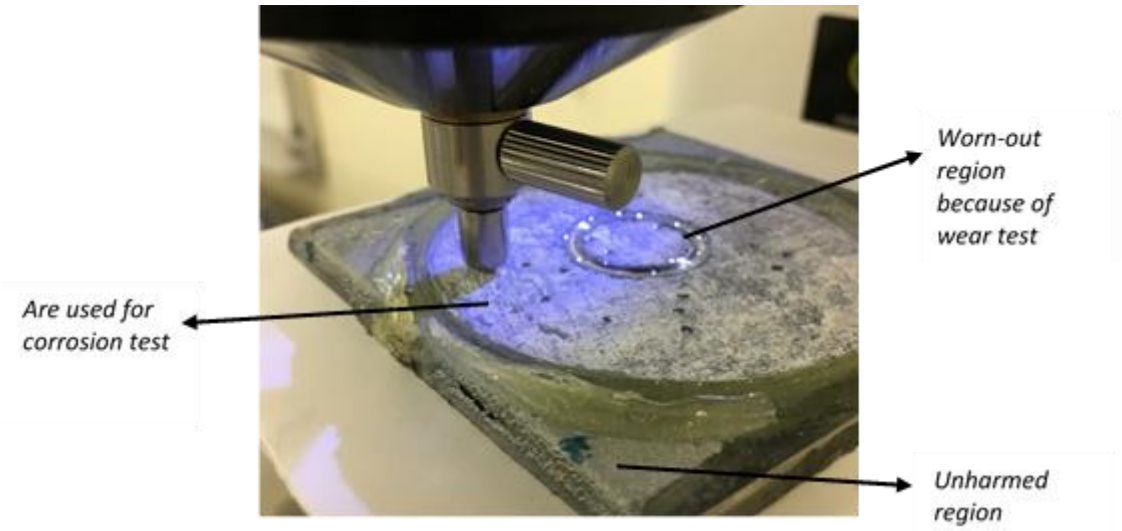

Figure A-1. Regions subjected to Rockwell hardness test.

Table A-2. Rockwell hardness results - Rockwell scale B (HRB).

Number of Test	**R1**	**R2**	**R3**
1	41.8	24.8	42.7
2	47.1	24.6	31.9
3	43.9	35	51.3
4	49.1	38.5	47.7
5	47.3	21.4	38.8
6	51.2	37.2	40.1
7	56.7	38.6	38.7
8	56.3	27.5	39.5
Average	49.17±5.36	30.95±7.09	41.33±5.96